ZFP451-mediated SUMOylation of SATB2 drives embryonic stem cell differentiation

Gustavo Antonio Urrutia,[1,5] Haribaskar Ramachandran,[1,5] Pierre Cauchy,[1,5] Kyungjin Boo,[1] Senthilkumar Ramamoorthy,[1] Soeren Boller,[1] Esen Dogan,[2] Thomas Clapes,[1] Eirini Trompouki,[1] Maria-Elena Torres-Padilla,[3] Jorma J. Palvimo,[4] Andrea Pichler,[2] and Rudolf Grosschedl[1]

[1]Department of Cellular and Molecular Immunology, Max Planck Institute of Immunobiology and Epigenetics, 79108 Freiburg, Germany; [2]Department of Epigenetics, Max Planck Institute of Immunobiology and Epigenetics, 79108 Freiburg, Germany; [3]Institute of Epigenetics and Stem Cells, Helmholtz Center Munich, 81377 Munich, Germany; [4]Institute of Biomedicine, University of Eastern Finland, 70210 Kuopio, Finland

The establishment of cell fates involves alterations of transcription factor repertoires and repurposing of transcription factors by post-translational modifications. In embryonic stem cells (ESCs), the chromatin organizers SATB2 and SATB1 balance pluripotency and differentiation by activating and repressing pluripotency genes, respectively. Here, we show that conditional *Satb2* gene inactivation weakens ESC pluripotency, and we identify SUMO2 modification of SATB2 by the E3 ligase ZFP451 as a potential driver of ESC differentiation. Mutations of two SUMO-acceptor lysines of *Satb2* (*Satb2*$^{K\rightarrow R}$) or knockout of *Zfp451* impair the ability of ESCs to silence pluripotency genes and activate differentiation-associated genes in response to retinoic acid (RA) treatment. Notably, the forced expression of a SUMO2-SATB2 fusion protein in either *Satb2*$^{K\rightarrow R}$ or *Zfp451*$^{-/-}$ ESCs rescues, in part, their impaired differentiation potential and enhances the down-regulation of *Nanog*. The differentiation defect of *Satb2*$^{K\rightarrow R}$ ESCs correlates with altered higher-order chromatin interactions relative to *Satb2*^{wt} ESCs. Upon RA treatment of *Satb2*^{wt} ESCs, SATB2 interacts with ZFP451 and the LSD1/CoREST complex and gains binding at differentiation genes, which is not observed in RA-treated *Satb2*$^{K\rightarrow R}$ cells. Thus, SATB2 SUMOylation may contribute to the rewiring of transcriptional networks and the chromatin interactome of ESCs in the transition of pluripotency to differentiation.

[*Keywords*: SATB2; SATB1; ZFP451; SUMO2; LSD1; ES cell; pluripotency; differentiation]

Supplemental material is available for this article.

Received October 16, 2020; revised version accepted June 8, 2021.

Embryonic stem cells (ESCs) are unique in their ability to differentiate into precursors of all three germ layers in response to external signals and cell-intrinsic cues (for review, see Martello and Smith 2014). The pluripotency of ESCs exist in three forms, termed naïve, formative, and primed, that represent distinct states toward lineage specification and differentiation (Smith 2017). Naïve, ground-state ESCs represent naïve preimplantation epiblasts. The formative state corresponds to early postimplantation epiblasts and characterizes ESCs before they remodel transcriptional, epigenetic, and metabolic networks for transit to the primed state in which ESCs acquire the expression of lineage-specifying factors and become responsive to differentiation cues (Weinberger et al. 2016; Kalkan et al. 2017; Smith 2017; Neagu et al. 2020). Primed state ESCs coexpress pluripotency and lineage-specifying transcription factors and are represented by epiblast-derived stem cells (EpiSCs), which have a reduced potential of chimera formation (Nichols and Smith 2009; Han et al. 2010). General pluripotency of ESCs is defined by the transcription factors (TFs) OCT4 (Pou5f1), SOX2, and SALL4, whereas naive pluripotency involves the additional expression of NANOG, KLF2, KLF4, ESRRB, and TBX3 (Kalkan et al. 2017, 2019). Formative pluripotency requires the down-regulation of naïve pluripotency factors and the expression of OTX2, OCT6 (Pou3f1), FGF5, and LEF1 (Acampora et al. 2016; Kalkan et al. 2019). Primed ESCs express the lineage-specifying factors FOXA2, SOX1, and Brachyury (T) (Nichols and Smith 2009; Hackett and Surani 2014).

NANOG plays an important role in ESC self-renewal by enabling the acquisition of both embryonic and induced pluripotency (Chambers et al. 2003; Mitsui et al. 2003;

[5]**These authors contributed equally to this work.**
Corresponding author: grosschedl@ie-freiburg.mpg.de
Article published online ahead of print. Article and publication date are online at http://www.genesdev.org/cgi/doi/10.1101/gad.345843.120.

Silva et al. 2009). Fluctuations of NANOG expression in ESCs, cultured in serum plus leukemia inhibitory factor (LIF), are associated with an altered predisposition to differentiate (Chambers et al. 2007; Torres-Padilla and Chambers 2014). Moreover, constitutive NANOG expression allows for LIF-independent self-renewal of ESCs (Chambers et al. 2003; Niwa et al. 2009). Pluripotency TFs can also be repurposed to support lineage-specific differentiation via changes in their relative abundance, interaction partners, and/or post-translational modifications (PTMs) (Wang et al. 2012; Ramakrishna et al. 2014; Heurtier et al. 2019). However, the mechanisms of repurposing TFs and regulators of higher-order chromatin during differentiation are not well understood.

The mammalian genome contains clusters of AT-rich sequences, termed matrix attachment regions (MARs), which have been involved in facilitating interactions between distal DNA elements and DNA looping (Tsutsui et al. 2005; Schneider and Grosschedl 2007). SATB1 and SATB2 are MAR-binding proteins that regulate gene expression by shaping chromatin architecture and recruiting chromatin remodelers (Yasui et al. 2002; Cai et al. 2006; Wang et al. 2014; Yang et al. 2015). In ES cells, SATB1 and SATB2 regulate mouse ESC pluripotency and *Nanog* expression in an antagonistic manner (Savarese et al. 2009). SATB1 deficiency impairs ESC differentiation and augments expression of *Nanog*, whereas a combined *Satb1*/*Satb2* double deficiency rescues these differentiation defects (Savarese et al. 2009). Moreover, the overexpression of SATB2 antagonizes differentiation-associated silencing of *Nanog* in ESCs and enhances heterokaryon-based reprogramming of human B lymphocytes (Savarese et al. 2009). SATB1/2-dependent regulation of *Nanog* has also been shown in the early mouse embryo (Goolam and Zernicka-Goetz 2017). Together, these observations suggest that the balance of SATB1 and SATB2 function regulates the choice between pluripotency and differentiation. However, the underlying mechanism of the antagonistic function of *Satb1* and *Satb2* remains obscure.

Interestingly, SATB proteins, which share a similar domain structure including DNA-binding CUT domains and an ubiquitin-like domain that allows for homotetramerization and heterotetramerization (Wang et al. 2014), differ in post-translational modifications. SATB1 is a target for phosphorylation and caspase cleavage (Galande et al. 2001), whereas SATB2 can be modified with the small ubiquitin-like modifier SUMO (Dobreva et al. 2003). Here, we found that SATB2 is modified with SUMO2 in RA-treated but not in LIF-cultured ESCs, and we identify ZFP451 as the functional SUMO E3 ligase. Moreover, we show that mutations of the two SUMO acceptor sites in SATB2 impair the differentiation potential of ESCs, which can be rescued, at least in part, by the forced expression of a SUMO2-SATB2 fusion protein. By combining these data with genome-wide ChIP-seq and RNA-seq analyses, we found that differentiation-induced SUMOylation of SATB2 enables a functional switch from promoting NANOG expression and pluripotency to enhancing differentiation by the down-regulation of pluripotency genes, enabling the occupancy of lineage-specific genes and the recruitment of the LSD1/CoREST complex.

Results

Satb2 *inactivation results in impaired ESC pluripotency and decreased NANOG expression*

The analysis of SATB2 function in ESCs pluripotency and differentiation has been hampered by the inability to generate ESCs from $Satb2^{-/-}$ embryos. Therefore, we examined whether SATB2-deficient ESCs could be generated by conditional inactivation of the *Satb2* gene. To this end, we generated ESCs from $Satb2^{fl/fl}$ $RERT^{Cre}$ embryos (Leone et al. 2015), and we treated the cells with tamoxifen to generate deleted $Satb2^{\Delta/\Delta}$ alleles. We confirmed successful deletion by immunoblot analysis and examined protein expression of the *Nanog* pluripotency gene, which we have previously shown to be bound and regulated by SATB1 and SATB2 (Fig. 1A). In LIF-cultured $Satb2^{\Delta/\Delta}$ ESCs, we detected a decrease in protein and mRNA expression of *Nanog* relative to the levels observed in $Satb2^{wt}$ cells (Fig. 1A,B). We also examined the morphology and alkaline phosphatase activity as general indicators of pluripotency in ESCs cultured in LIF or treated with retinoic acid (RA) to induce differentiation. In LIF-cultured $Satb2^{\Delta/\Delta}$ ESCs, we observed an enhanced frequency of cells with a differentiated morphology relative to $Satb2^{wt}$ cells, which was further increased upon RA treatment (Fig. 1C). Together, these data suggest that the conditional inactivation of *Satb2* impairs ESC pluripotency. In this analysis, we noted an increase of SATB2 expression in RA-treated cells that can be accounted for by a concomitant increase in *Satb2* transcript levels (Fig. 1B; Savarese et al. 2009). Moreover, the appearance of a slower migrating form of SATB2 in RA-treated ESCs raised the question of whether post-translational modification of SATB2 allows for a functional repurposing during differentiation.

SUMO2 modification of SATB2 during ESC differentiation

We have previously shown that ectopically expressed SATB2 can be SUMO-modified at lysines K233 and K350 in Hek293T cells and in vitro by the SUMO E3 ligase PIAS1 (Dobreva et al. 2003). Therefore, we examined whether SUMOylation of endogenous SATB2 can be detected in self-renewing murine ESCs and/or in ESCs that have been induced to differentiate by treatment with RA. Immunoblot analysis of cell lysates in the absence or presence of *N*-ethylmaleimide (NEM) to preserve SUMO modifications indicated that SATB2 protein is detected as a single band at ~100 kDa in LIF-cultured pluripotent cells (Fig. 1D). During RA treatment, the abundance of SATB2 increased concomitantly with the appearance of a higher-molecular-weight band of ~130 kDa (Fig. 1D). In RA-treated cells, we also detected a faster-migrating form of SATB2 (~70 kD) that is generated by alternative promoter usage (data not shown). To examine whether

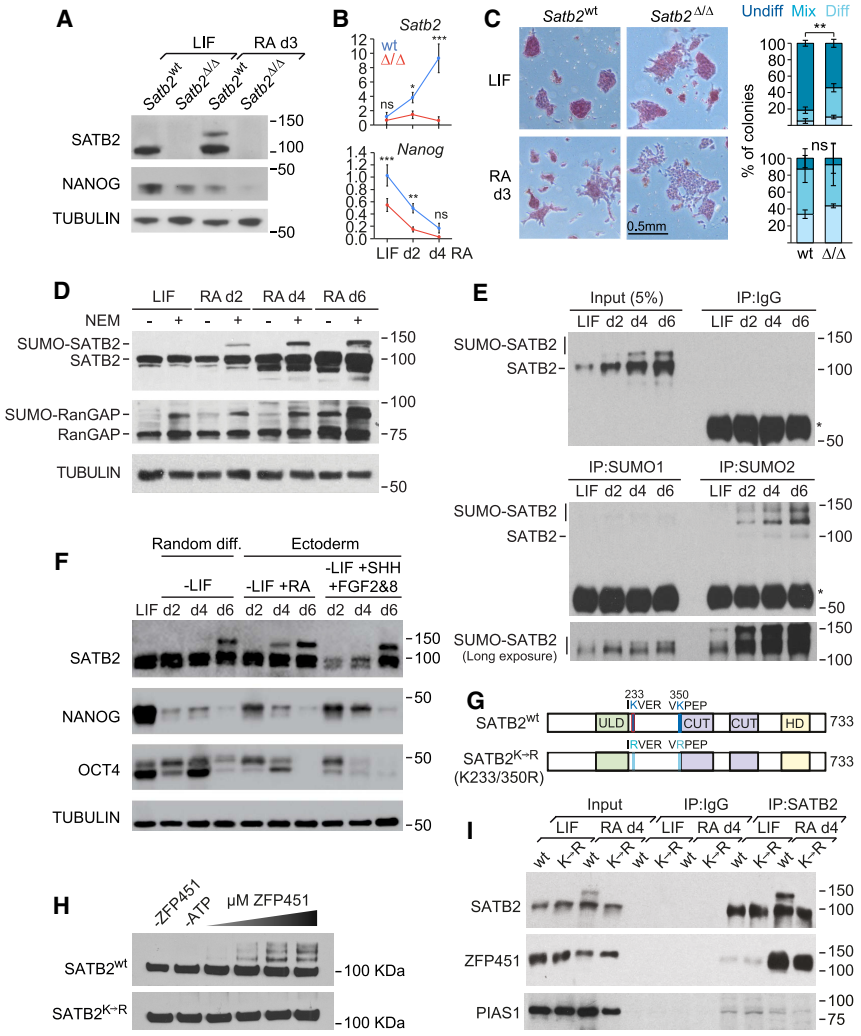

Figure 1. SUMOylation of SATB2 during ESC differentiation toward ectodermal progenitors. (*A*) Immunoblots detecting SATB2, NANOG, and TUBULIN in wild-type (*Satb2*^{wt}) and Satb2-deficient (*Satb2*$^{\Delta/\Delta}$) ESCs, cultured in LIF or with retinoic acid (RA) for 2 or 4 d. Blots were generated with ESCs from *Satb2*^{wt} clone 8 and *Satb2*$^{\Delta/\Delta}$ clone 2. Data are representative for three independently derived *Satb2*^{wt} clones (8, 24.1, and 24.3) and *Satb2*$^{\Delta/\Delta}$ clones (2, 32, and 64). *Satb2*$^{\Delta/\Delta}$ ESCs were generated by treatment of *Satb2*$^{fl/fl}$*Cre*$^{ERT/+}$ ESCs with 10 μM tamoxifen for 5 d. All clones were cultured on fibronectin-coated dishes before replating onto gelatin-coated dishes for differentiation. (*B*) qRT-PCR analysis to detect *Satb2* and *Nanog* transcripts in LIF-cultured or RA-treated (d2 and d4) *Satb2*^{wt} and *Satb2*$^{\Delta/\Delta}$ ESCs. Values are derived from three clones each and are calculated relative to those of *Satb2*^{wt} clone 24.1 in LIF and normalized to *Pgk*. (*C*) Alkaline phosphatase staining and quantification of *Satb2*^{wt} and *Satb2*$^{\Delta/\Delta}$ ESCs cultured in LIF or RA for 3 d. The percentages of undifferentiated, differentiated, and mixed-type colonies are indicated in the bar plot. Images are representative of two independent experiments carried out with each clone. Values in *B* and *C* are expressed as the combined mean ± SD of all clones from either genotype. *t*-tests were carried out relative to *Satb2*$^{+/+}$ cells. Significance levels are as follows: (*) $P < 0.05$, (**) $P < 0.01$, (***) $P < 0.001$. (*D*) Immunoblots detecting SATB2 and RanGAP in ESCs, cultured in LIF or with retinoic acid (RA) for 2, 4, or 6 d. Whole-cell lysates were purified in the presence (+) or absence (−) of the SUMO-isopeptidase inhibitor NEM (10 mM). SUMO-modified forms of SATB2 and RanGAP are marked. RanGAP was used as a positive control for SUMOylation, and Tubulin was used as a loading control. (*E*) Immunoblots of endogenous SATB2 that was immunoprecipitated (IP) with mouse anti-IgG, bead-coupled anti-SUMO1, or anti-SUMO2 antibodies and eluted with SUMO1 or SUMO2 peptides. Cell culture conditions were as in *A*. The asterisk indicates the IgG bands of antibodies used in the IP. (*F*) Immunoblot analysis of whole-cell extracts from wild-type ESCs randomly differentiated (−LIF) and toward ectoderm using two distinct protocols. Blots were probed with antibodies to detect indicated proteins. Ectoderm differentiation was induced by LIF withdrawal and addition of RA, or by the addition of FGF2, FGF8, and SHH. (*G*) Schematic representation of SATB2 protein, highlighting the SUMO consensus motifs at K233 and K350 in SATB2^{wt} and the arginine substitutions (K → R) in the double-mutant SATB2$^{K\rightarrow R}$. (*H*) Immunoblots of an in vitro SUMOylation assay using recombinant purified SATB2^{wt}, SATB2$^{K\rightarrow R}$, and increasing amounts of recombinant ZFP451protein (amino acids 2–246), comprising SUMO E3 activity (Eisenhardt et al. 2015). (*I*) Coimmunoprecipitation of SATB2 to detect interaction with ZFP451 and PIAS1 in *Satb2*^{wt} (wt) or *Satb2*$^{K\rightarrow R}$ ESCs cultured in LIF or in RA for 4 d. Immunoblots are representative of three or four independent experiments using wt clones DV3 and C2 (*A*,*B*) and *Zfp451*$^{+/+}$ clone 14 (*B*). In vitro SUMOylation immunoblot is representative of three independent experiments.

the ~130-kDa band corresponds to SUMO-SATB2, we immunoprecipitated endogenously SUMOylated proteins with anti-SUMO1 or anti-SUMO2 antibodies and visualized SATB2 proteins by immunoblot analysis (Fig. 1E). SUMO1-SATB2 was detected at low levels in both pluripotent and differentiating ESCs, whereas SUMO2-SATB2 was strongly enriched in differentiating ESCs.

To determine whether SATB2 SUMOylation is triggered by differentiation rather than by RA signaling, we induced random differentiation by LIF withdrawal and ectodermal differentiation by the addition of FGF2, FGF8, and SHH (Supplemental Fig. S1A; Ying et al. 2003). The dynamics of SATB2 SUMOylation and protein and mRNA expression during ectodermal differentiation were similar, regardless of the signaling pathways used for differentiation (Fig. 1F; Supplemental Fig. S1B,C). Successful differentiation was also assessed by the analysis of NANOG, OCT4, NESTIN, PAX6, and SOX1 protein expression (Supplemental Fig. S1C). The lack of SATB2 detection in *Satb1*$^{-/-}$*Satb2*$^{-/-}$ (Savarese et al. 2009) and *Satb2*$^{\Delta/\Delta}$ ESCs confirmed the specificity of the anti-SATB2 antibody (Fig. 1A; Supplemental Fig. S1C). Heat or

proteotoxic stress, which is known to activate the SUMO machinery (Enserink 2015), did not lead to SUMOylation of SATB2 despite induced global SUMO conjugation (Supplemental Fig. S1D). Therefore, the modification of SATB2 with SUMO2 is specifically triggered during differentiation.

The SUMO E3 ligase ZFP451 interacts with SATB2 specifically in differentiating ESCs

To understand the developmental regulation of SATB2 SUMOylation, we aimed to identify the SUMO E3 ligase that mediates this modification. ZNF451 (murine ZFP451) has been identified as an E2- and SUMO-interacting protein (Karvonen et al. 2008) and was recently characterized as a bone fide SUMO E3 ligase with a marked preference for SUMO2 conjugation (Cappadocia et al. 2015; Eisenhardt et al. 2015). Moreover, a mass spectrometry screen identified SATB2 as a potential target of ZNF451 in HEK293 cell extracts (JJ Palvimo, unpubl.). To examine whether ZFP451 can mediate SUMOylation of SATB2, we performed an in vitro SUMOylation assay. To this end, we used a recombinant ZFP451 fragment carrying E3 activity (Eisenhardt et al. 2015) and recombinant wild-type SATB2 or mutant SATB2 ($SATB2^{K\rightarrow R}$) in which the SUMO acceptor lysines 233 and 350 had been replaced by arginines (Fig. 1G; Supplemental Fig. S1E; Dobreva et al. 2003). We detected SUMOylation of wild-type but not mutant SATB2 protein in a dose-dependent manner, indicating that SATB2 is a substrate for ZFP451 (Fig. 1H). Moreover, we examined the interaction of endogenous SATB2 or $SATB2^{K\rightarrow R}$ with ZFP451 by coimmunoprecipitations in lysates of pluripotent and differentiating ESCs. We detected a strong interaction of SATB2 but not $SATB2^{K\rightarrow R}$ with ZFP451 specifically in lysates of RA-treated ESCs (Fig. 1I). The expression of ZFP451 was similar in pluripotent and differentiating ESCs (Supplemental Fig. S1F). We also detected weak interactions of SATB2 with the PIAS1 SUMO E3 ligase in lysates of both pluripotent and differentiating ES cells Supplemental Fig. S1F). Thus, ZFP451 could be the E3 ligase responsible for the SUMO2 modification of SATB2 during RA-induced differentiation.

Loss of SATB2 SUMOylation in ZFP451-deficient ESCs

To further examine the function of ZFP451 as an E3 ligase that mediates SUMOylation of SATB2 in differentiating ESCs, we knocked down the isoforms 1 and 2 of *Zfp451* with specific shRNAs. Immunoblot analysis revealed a marked decrease of ZFP451 expression in *Zfp451* KD cells relative to control KD transduced with scrambled shRNA (Supplemental Fig. S2A). Analysis of SATB2 protein expression in RA-treated *Zfp451* KD cells indicated that the SUMOylated forms of SATB2 cannot be detected even at day 6 of differentiation (Supplemental Fig. S2B). In contrast, the global levels of SUMO1- and SUMO2-conjugated proteins were not significantly altered in *Zfp451* KD cells relative to controls (Supplemental Fig. S2C). We further generated mice carrying a $Zfp451^{tm1a(EUCOMM)}$ knockout allele ($Zfp451^{+/-}$) and derived $Zfp451^{+/+}$, $Zfp451^{+/-}$, and $Zfp451^{-/-}$ ESC lines. Immunoblot analysis confirmed that three independent $Zfp451^{-/-}$ clones with normal karyotypes had no detectable ZFP451 protein expression (Fig. 2A; Supplemental Fig. S2D,E). In differentiating $Zfp451^{+/-}$ and $Zfp451^{-/-}$ ESCs, we detected reduced and no SUMOylation of SATB2, respectively (Fig. 2A). However, the *Zfp451* deletion did not affect the overall increase in SATB2 protein levels during RA-induced differentiation (Fig. 2A). Together, these data show that ZFP451 mediates the SUMOylation of SATB2 during RA-induced differentiation of ESCs.

Impaired differentiation of $Zfp451^{-/-}$ *and* $Satb2^{K\rightarrow R}$ *ESCs*

We then examined whether ESC differentiation is impaired in $Zfp451^{-/-}$ and $Satb2^{K\rightarrow R}$ ESCs. In $Zfp451^{-/-}$ and *Zfp451* KD cells, we noted an impaired differentiation of the cells upon RA treatment, as quantified by staining with alkaline phosphatase (Fig. 2B; Supplemental Fig. S2F). Moreover, immunoblot analysis indicated that NANOG protein levels were only modestly reduced in RA-treated $Zfp451^{-/-}$ and *Zfp451* KD ESCs, confirming their impaired differentiation (Fig. 2A; Supplemental Fig. S2B). To examine whether the lack of SATB2 SUMOylation during RA treatment of $Zfp451^{-/-}$ ESCs accounts for their differentiation defect, we also analyzed $Satb2^{K\rightarrow R}$ ESCs. In LIF conditions, $Satb2^{K\rightarrow R}$ ESCs showed no obvious differences with $Satb2^{wt}$ cells in terms of morphology and NANOG expression (Fig. 2C,D). Upon RA treatment of $Satb2^{K\rightarrow R}$ ESCs, we observed an up-regulation of SATB2 protein levels but did not detect any SUMO-SATB2 forms (Fig. 2C). $Satb2^{K\rightarrow R}$ ESCs showed marked and consistent defects in the down-regulation of NANOG and up-regulation of NESTIN even after 6 d of culture in RA (Fig. 2C; Supplemental Fig. S2G). Moreover, the majority of $Satb2^{K\rightarrow R}$ cells stained as AP-positive and retained a high percentage of undifferentiated and mixed colonies compared with $Satb2^{wt}$ cultures after 3 d in RA culture (Fig. 2D). Consistent with a differentiation defect, we also observed enhanced proliferation with no change in apoptosis of RA-treated $Satb2^{K\rightarrow R}$ and $Zfp451^{-/-}$ ESCs, relative to their control counterparts (Supplemental Fig. S2H,I).

SUMO2 modification of SATB2 is required for RA-induced ESC differentiation

To establish a direct link between SATB2 SUMOylation and the differentiation defect of $Satb2^{K\rightarrow R}$ and $Zfp451^{-/-}$ cells, we examined the potential of an N-terminal SUMO-fusion of $SATB2^{K\rightarrow R}$ to rescue the differentiation defects (Fig. 2E). To this end, we complemented $Satb2^{K\rightarrow R}$ and $Zfp451^{-/-}$ cells with a FLAG- SUMO2-FLAG-$Satb2^{K\rightarrow R}$ (termed SUMO2-Satb2) vector or with a FLAG-Satb2 (termed Satb2) vector as control by transfection and analyzed these cells in terms of morphology and expression of pluripotency and lineage-specific markers (Fig. 2F–H). Immunoblot analysis of the complemented

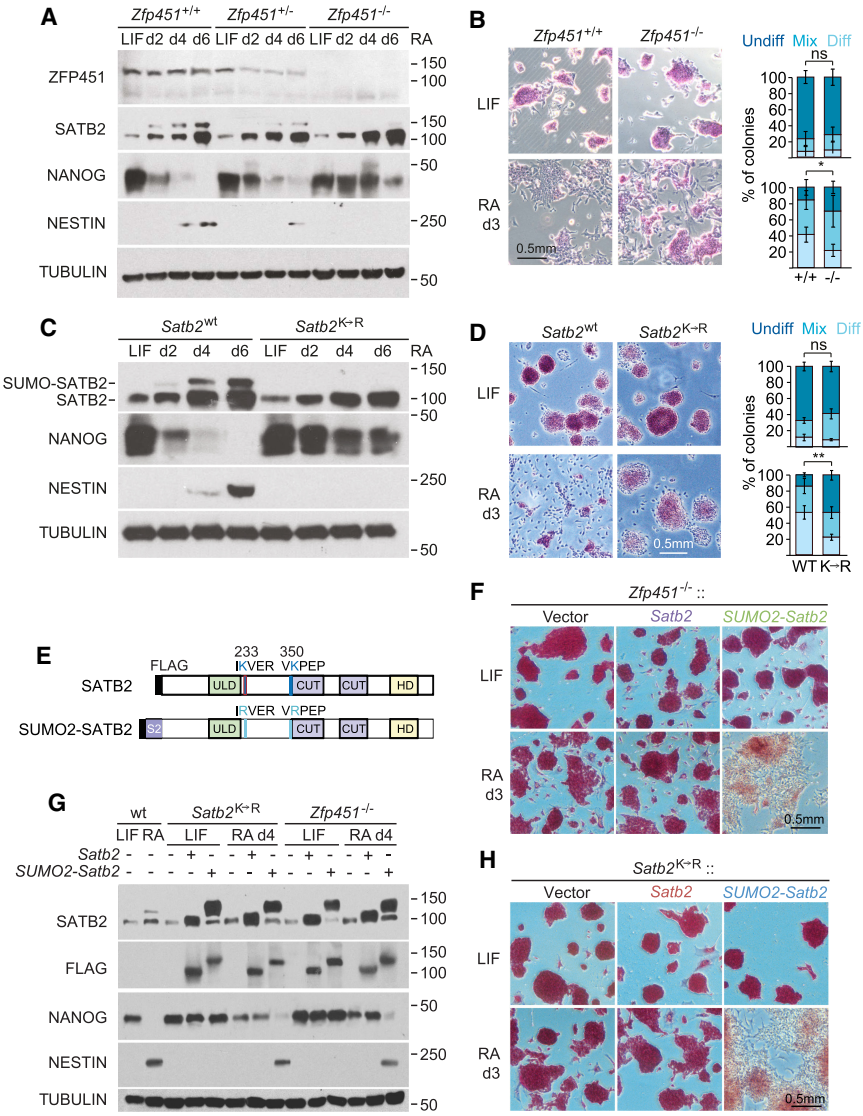

Figure 2. Impaired differentiation of SUMO-SATB2-deficient cells. (*A*) Immunoblot analysis to detect ZFP451, SATB2, NANOG, NESTIN, and TUBULIN in whole-cell extracts from *Zfp451*$^{+/+}$, *Zfp451*$^{+/-}$, and *Zfp451*$^{-/-}$ ESCs cultured in pluripotent conditions (LIF) or differentiated with RA for 2, 4, and 6 d. (*B*) Alkaline phosphatase staining and quantification of *Zfp451*$^{+/+}$ and *Zfp451*$^{-/-}$ ESCs cultured in LIF or RA for 3 d. The percentage of undifferentiated, differentiated, and mixed type colonies are indicated in the bar plot. (*C*,*D*) Immunoblot analysis and alkaline phosphatase staining of *Satb2*^{wt} and *Satb2*$^{K\rightarrow R}$ ESCs as described in *A* and *B*. In the bar plots of *B* and *D*, triplicate data are represented as mean ± SD, and the statistical significant differences calculated by paired *t*-tests are indicated as follows: (ns) nonsignificant, (*) $P < 0.05$, or (**) $P < 0.01$. (*E*) Schematic representation of FLAG-SATB2^{wt} (termed SATB2) and FLAG-SUMO2-Satb2$^{K\rightarrow R}$ (termed SUMO2-SATB2) proteins. (*F*) Alkaline phosphatase staining of *Zfp451*$^{-/-}$ ESCs transfected with empty vector, SATB2-expressing, or SUMO2-SATB2-expressing plasmids. Cells were cultured in LIF or in RA for 3 d (for quantification, see Supplemental Fig. S3C). (*G*) Immunoblot analysis to detect SATB2, FLAG-tagged SATB2, ZFP451, NANOG, NESTIN, and TUBULIN in ESC cultures as described in *B*. The dash indicates transfection with empty vector. (*H*) Alkaline phosphatase staining of *Satb2*$^{K\rightarrow R}$ ESCs transfected with empty vector, SATB2-expressing, or SUMO2-SATB2-expressing plasmids. Cells were cultured in LIF or in RA for 3 d (for quantification, see Supplemental Fig. S3D). Immunoblots and alkaline phosphate staining are representative of three independent experiments, using *Satb2*^{wt} clones C1 and C2; *Zfp451*$^{+/+}$ clone 14; *Zfp451*$^{-/-}$ clones 4, 7, and 10; and *Zfp451*$^{+/-}$ clones 11 and 13.

ES cell clones showed abundant and equivalent expression of SUMO2-SATB2 and SATB2 proteins (Fig. 2G). Moreover, the stability of both overexpressed and endogenous SATB2 and SUMO-SATB2 proteins were similar (Supplemental Fig. S3A,B). As expected, ectopically expressed SATB2 was not SUMO-modified in RA-treated *Zfp451*$^{-/-}$ cells (Fig. 2G). However, the exogenous SATB2 protein was also not SUMOylated in RA-treated ZFP451-expressing *Satb2*$^{K\rightarrow R}$ cells, potentially because of a steric hindrance by the FLAG tag or because of a stabilization of pluripotency by the overexpression of SATB2 prior to differentiation. Thus, SATB2 overexpression did not significantly alter the morphology and AP staining of cells in LIF and RA conditions (Fig. 2F,H; Supplemental Fig. S3C,D). In both *Satb2*$^{K\rightarrow R}$ and *Zfp451*$^{-/-}$ cells, however, the ectopic expression of SUMO2-SATB2 resulted in a reduced AP staining and the acquisition of a differentiated morphology, albeit to a lesser extent than wild-type controls (Fig. 2F,H; Supplemental Fig. S3C,D). No significant changes in morphology were observed in LIF conditions, suggesting that the expression of SUMO2-SATB2 is necessary but not sufficient to induce a differentiated phenotype. SATB2-complemented cells continued to express relatively high levels of NANOG after induction of differentiation, whereas SUMO-SATB2-complemented cells showed markedly reduced NANOG levels (Fig. 2G). The restored down-regulation of *Nanog* and up-regulation of the differentiation marker *Rai2* in SUMO2-SATB2-expressing *Satb2*$^{K\rightarrow R}$ and *Zfp451*$^{-/-}$ cells were confirmed by qRT-PCR analysis (Supplemental Fig. S3E). Together, these data suggest that the loss of SUMOylation of SATB2 is responsible for the differentiation defects of *Satb2*$^{K\rightarrow R}$ and *Zfp451*$^{-/-}$ cells, although a final proof would require the expression of a SUMO2-SATB2 protein from the endogenous *Satb2* locus.

Zfp451$^{-/-}$ and Satb2$^{K \to R}$ ESCs can transit to the primed state of pluripotency

The question arose as to whether *Satb2*$^{K \to R}$ and *Zfp451*$^{-/-}$ ESCs can transit to the primed state of pluripotency. Epiblast stem cells (Epi-SCs) correspond to the "primed" state of the postimplantation epiblast, and they differ from ESCs by their inefficiency of chimera formation and requirement of FGF and Activin A signaling for self-renewal (Han et al. 2010; Lanner and Rossant 2010). Epi-SCs express *Oct4*, *Sox2*, and *Nanog* along with *Fgf5* and *Brachyury* (T), and they can be generated as stable intermediates before differentiation of ESCs into the germ layers (Han et al. 2010). To examine whether the deficiency of Satb2 SUMOylation affects the transition of ESCs to Epi-SCs, we treated *Satb2*$^{K \to R}$ and *Zfp451*$^{-/-}$ ESCs with FGF and Activin A. Immunoblot analysis indicated that both mutant cells are able to down-regulate REX1 (Zfp42) and up-regulate FGF5 while maintaining the expression of NANOG, suggesting that the cells were able to transit to an Epi-SC state (Fig. 3A). This observation was confirmed by analysis of the cell morphology and up-regulation of *Otx2* mRNA (Fig. 3B; Supplemental Fig. S3F).

We also assessed the ability of *Satb2*^{wt}, *Satb2*$^{K \to R}$, and *Zfp451*$^{-/-}$ ESCs to participate in the formation of chimeric embryos. Toward this end, we stably transfected cells with a tdTomato reporter gene and confirmed expression by antibody staining and flow cytometry (Fig. 3C). TdTomato-positive ESCs were injected into 16-cell stage embryos (morulae), and embryos were collected at E10.5. TdTomato-expressing cells were detected in 12/33 embryos that were derived from morulae injected with *Satb2*^{wt} ESCs, whereas virtually no tdTomato-positive cells were detected in embryos derived from morulae injected with *Satb2*$^{K \to R}$ or *Zfp451*$^{-/-}$ ESCs (Fig. 3C). To examine whether the impaired contribution of *Satb2*$^{K \to R}$ and *Zfp451*$^{-/-}$ ESCs to chimera is due to increased apoptosis, we performed tunnel assays on aggregated E4.5 morulae. By immunofluorescence analysis, we did not detect an increase of apototic cells in morulae containing tdTomato-positive *Satb2*$^{K \to R}$ or *Zfp451*$^{-/-}$ cells relative to *Satb2*^{wt} cells (Supplemental Fig. S3G). Taken together, these data suggest that ESCs in which SATB2 is not properly SUMOylated have a reduced potential for chimera formation.

Altered chromatin interactions at the Nanog locus in RA-treated Satb2$^{K \to R}$ and Zfp451$^{-/-}$ ESCs

During RA-induced differentiation, the *Nanog* locus has been shown to undergo changes in its 3D configuration (Apostolou et al. 2013). Since the tetrameric SATB proteins have been implicated in the formation of chromatin loops (Dickinson et al. 1997; Cai et al. 2006; Galande et al. 2007; Wang et al. 2014; Yamasaki and Yamasaki 2016; Ghosh et al. 2019), we hypothesized that chromatin conformation of the *Nanog* locus could also be affected by SATB2 SUMOylation. Therefore, we performed 3C assays to analyze interactions between the promoter, −5-kb enhancer, and +12-kb element of the *Nanog* locus in *Satb2*$^{K \to R}$, *Zfp451*$^{-/-}$, and *Satb2*^{wt} ESCs under LIF and RA conditions. This analysis revealed reduced interactions between these regulatory elements in RA-treated *Satb2*^{wt} ESCs but only modest or no changes in

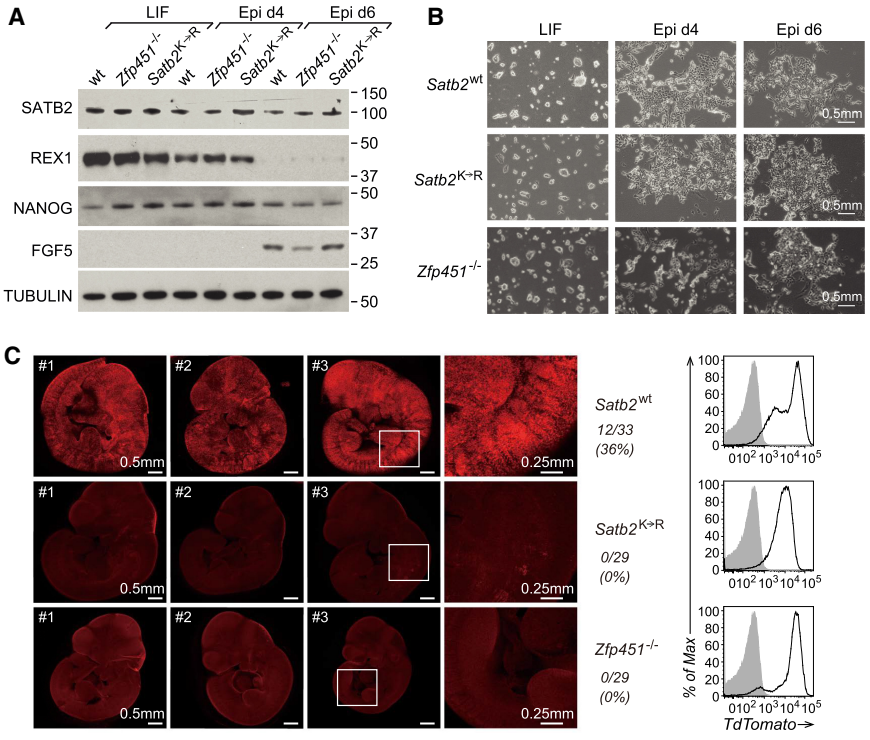

Figure 3. Loss of SATB2 SUMOylation allows for transition to primed pluripotency but impairs whole-embryo chimerism. (*A*) Immunoblot analysis of lysates from ESCs grown in LIF or in epiblast differentiation conditions to detect pluripotency and epiblast stem cell markers. (*B*) Morphology of *Satb2*^{wt}, *Satb2*$^{K \to R}$, and *Zfp451*$^{-/-}$ ESCs in LIF cultures or in epiblast differentiation conditions at d4 and d6. (*C*) Immunohistochemical detection of the chimeric contribution of tdTomato-expressing *Satb2*^{wt}, *Satb2*$^{K \to R}$, and *Zfp451*$^{-/-}$ cells in E10.5 embryos derived from ESC injections into morulae. The images of three embryos each are shown. The white squares indicate areas of embryos that are enlarged at the *right*. The frequencies and numbers of chimeric/total embryos are indicated. The *right* panels show the flow cytometric quantitation of tdTomato expression in *Satb2*^{wt}, *Satb2*$^{K \to R}$, and *Zfp451*$^{-/-}$ mESCs prior to the injection into morulae.

RA-treated *Satb2*$^{K\rightarrow R}$ and *Zfp451*$^{-/-}$ ESCs relative to LIF-cultured *Satb2*^{wt} ESCs (Fig. 4A,B). We have previously shown that SATB proteins bind to a region 11 kb upstream of the *Nanog* transcription start site (Savarese et al. 2009), and therefore, we included an analysis of the interactions of SATB-binding sites (BSs) with the other regulatory elements of the *Nanog* locus. This analysis indicated that the chromatin interactions detected in LIF-cultured cells are largely maintained in RA-treated *Satb2*$^{K\rightarrow R}$ and *Zfp451*$^{-/-}$ ESCs (Fig. 4C), which is consistent with the impaired down-regulation of NANOG protein expression in the mutant cells.

To extend the analysis of chromatin interactions, we performed genome-wide HiC assays on LIF-cultured *Satb2*^{wt} ESCs and RA-treated *Satb2*^{wt} and *Satb2*$^{K\rightarrow R}$ ESCs. We computed significant interactions and observed a higher overlap of interaction anchors as well as global correlation between LIF-cultured *Satb2*^{wt} and RA-treated Satb2$^{K\rightarrow R}$ ESCs than with RA-treated Satb2^{wt} ESCs (Fig. 4D; Supplemental Fig. S4A,B). To determine whether the interactions were changing at SATB2-occupied sites, we overlapped the union of interactions with SATB2-binding sites and retrieved interaction values from normalized HiC matrices. Strikingly, we observed that the genome-wide compartmentalization of SATB2-binding sites in RA-treated *Satb2*$^{K\rightarrow R}$ ESCs was more similar to that in LIF-cultured *Satb2*^{wt} than that in RA-treated *Satb2*^{wt} ESCs (Fig. 4E). We also confirmed that the interactions on chromosomes 6 and 4, containing the *Nanog* and *Foxd3* loci, respectively, were reduced in RA-treated *Satb2*^{wt} ESCs as compared with RA-treated *Satb2*$^{K\rightarrow R}$ ESCs (Fig. 4F,G; Supplemental Fig. S4C,D). Taken together, these data indicate that differentiation-induced changes of chromatin conformation near SATB2-binding sites are reduced in *Satb2*$^{K\rightarrow R}$ ESCs.

Overlapping and specific patterns of gene expression in Zfp451$^{-/-}$ *and* Satb2$^{K\rightarrow R}$ *ESCs*

To gain insight into the molecular basis of the impaired differentiation potential of *Zfp451*$^{-/-}$ and *Satb2*$^{K\rightarrow R}$ ESCs, we performed RNA-seq analysis in LIF-cultured and RA-treated ESCs. Overall, the gene expression pattern of *Zfp451*$^{-/-}$ ESCs resembled more closely wild-type (wt) ESCs than *Satb2*$^{K\rightarrow R}$ cells in LIF conditions but showed a pattern intermediary between wt and *Satb2*$^{K\rightarrow R}$ cells in RA conditions (Supplemental Fig. S5A,B). LIF-cultured *Zfp451*$^{-/-}$ and *Satb2*$^{K\rightarrow R}$ cells showed distinct changes in gene expression relative to wt cells, whereby a larger set of genes was dysregulated in *Zfp451*$^{-/-}$ ESCs as compared with *Satb2*$^{K\rightarrow R}$ ESCs (Fig. 5A–C; Supplemental Tables S1, S2). We thus generated lists of up- and down-regulated genes for *Zfp451*$^{-/-}$ and *Satb2*$^{K\rightarrow R}$ ESCs relative to the respective controls and compared them among each other.

In LIF conditions, a small but significant number of genes were up-regulated or down-regulated in both *Zfp451*$^{-/-}$ and *Satb2*$^{K\rightarrow R}$ ESCs (Fig. 5C; Supplemental Table S3). The expression of pluripotency genes (*Pou5f1*, *Sox2*, *Nanog*, *Esrrb*, and *Klf2*) was not altered in *Zfp451*$^{-/-}$ and *Satb2*$^{K\rightarrow R}$ cells relative to wild-type cells (Fig. 5D). In *Zfp451*$^{-/-}$ ESCs, however, genes associated with "primed" pluripotency/early implantation (*Fgf5*, *Lef1*, *Otx2*, *Pou3f1*, and *T*) and several lineage-priming genes (*Gata4*, *Gata6*, and *Sox17*) were dysregulated, whereas the expression of most of these genes was not altered in *Satb2*$^{K\rightarrow R}$ ESCs (Fig. 5D).

Upon RA treatment, we observed a large overlap of dysregulated genes in *Zfp451*$^{-/-}$ and *Satb2*$^{K\rightarrow R}$ cells (Fig. 5A–C). Although genes of naïve pluripotency failed to be down-regulated in both RA-treated *Satb2*$^{K\rightarrow R}$ and *Zfp451*$^{-/-}$ cells, general pluripotency genes failed to be down-regulated only in *Satb2*$^{K\rightarrow R}$ cells, whereas *Zfp451*$^{-/-}$ cells displayed a partial down-regulation of these genes (Fig. 5D). In both RA-treated *Satb2*$^{K\rightarrow R}$ and *Zfp451*$^{-/-}$ cells, many lineage-priming genes (*Foxa2*, *Gata4*, *Gata6*, and *Sox17*) were down-regulated relative to wt cells. Gene ontology analysis indicated that WNT and TGF-β signaling pathway genes are preferentially down-regulated in RA-treated *Satb2*$^{K\rightarrow R}$ ESCs, whereas metabolism and the pluripotency network genes are up-regulated in both *Satb2*$^{K\rightarrow R}$ and *Zfp451*$^{-/-}$ ESCs (Supplemental Fig. S5C). Additionally, we performed gene set enrichment analysis (GSEA) (Subramanian et al. 2005). *Zfp451*$^{-/-}$ and *Satb2*$^{K\rightarrow R}$ dysregulated gene signatures were enriched for genes down-regulated in "late" ESCs from embryoid bodies (EBs) as compared with "early" ESCs (Hailesellasse Sene et al. 2007), whereas EB-up-regulated genes were enriched in wt ESCs (Supplemental Fig. S5D). Collectively, the molecular analysis confirms the functional phenotypes of *Satb2*$^{K\rightarrow R}$ and *Zfp451*$^{-/-}$ ESCs. The RA-induced differentiation defect and the impaired down-regulation of pluripotency genes were more pronounced in *Satb2*$^{K\rightarrow R}$ ESCs than in *Zfp451*$^{-/-}$ ESCs, possibly due to a partial redundancy of ZFP451 with other SUMO E3 ligases. Therefore, we focused on the *Satb2*$^{K\rightarrow R}$ ESCs for our next analysis.

SUMOylation affects chromatin binding of SATB2

To identify direct SATB2 target genes, we analyzed the chromatin binding of SATB2^{wt} and SATB2$^{K\rightarrow R}$ in pluripotent and differentiating ESCs. To enhance the specificity and efficiency of chromatin immunoprecipitation, we added a 3xTy1 epitope-tag on the C terminus of the endogenous SATB2^{wt} and SATB2$^{K\rightarrow R}$ by CRISPR/Cas9-mediated editing. *Ty1-Satb2*^{wt} and *Ty1-Satb2*$^{K\rightarrow R}$ cells showed molecular phenotypes indistinguishable from their untagged counterparts (Supplemental Fig. S6A). In LIF-cultured ESCs, ChIP-seq of Ty1-tagged SATB2^{wt} and SATB2$^{K\rightarrow R}$ revealed 62 SATB2^{wt}-specific and 191 SATB2$^{K\rightarrow R}$-specific peaks (Fig. 6A, left; Supplemental Fig. S6B). In RA-cultured cells, we detected 657 SATB2^{wt}-specific and 159 SATB2$^{K\rightarrow R}$-specific occupancies, suggesting that the pronounced gain of SATB2 occupancy in the RA condition is specific for SATB2^{wt} (Fig. 6A, right; Supplemental Fig. S6B). We also compared the SATB2^{wt} occupancy in LIF- versus RA-cultured ESCs and also identified a large cluster of 701 sites with enhanced occupancy in RA-treated cells (RA-specific

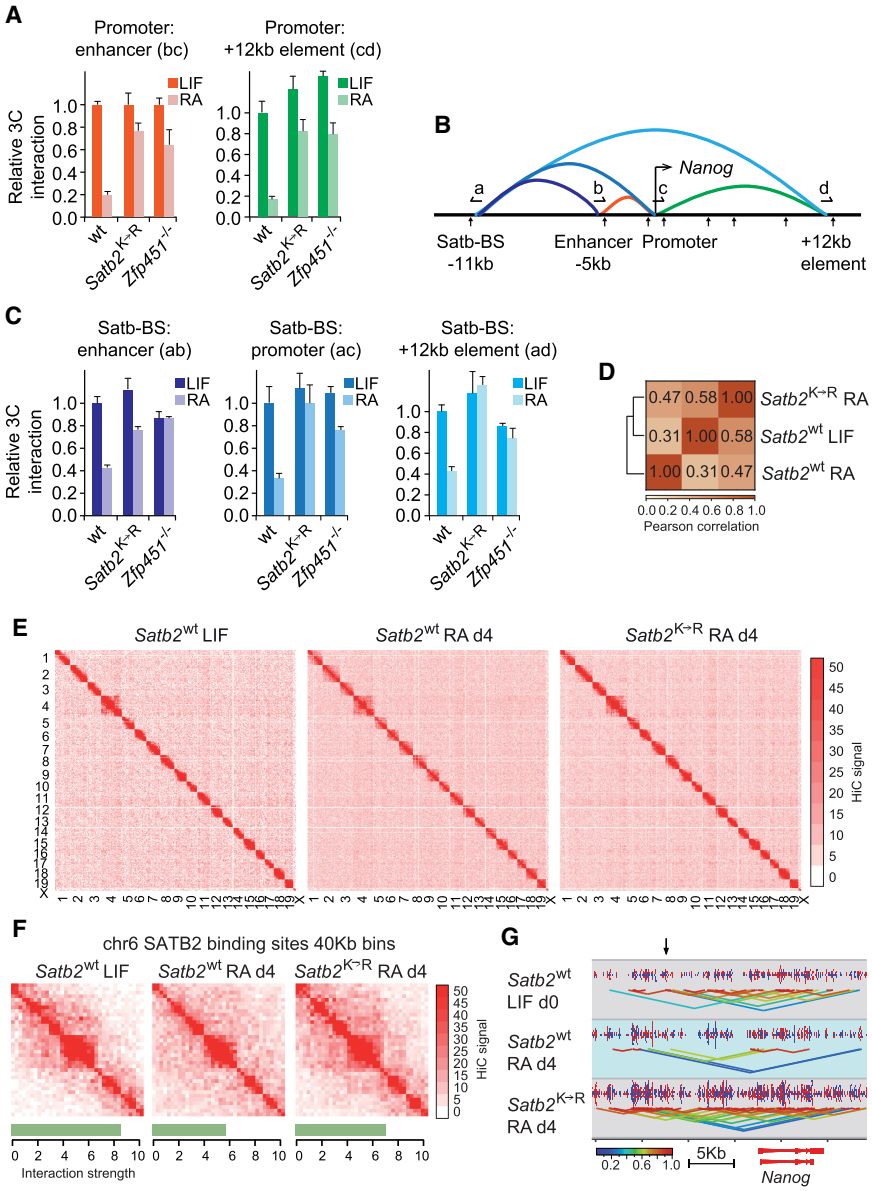

Figure 4. Loss of Satb2 SUMOylation alters long-range chromatin interactions. (*A*) 3C assays to detect interactions of *Nanog* promoter with the *Nanog* enhancer and the 12-kb downstream region in $Satb2^{wt}$, $Satb2^{K\rightarrow R}$, and $Zfp451^{-/-}$ ESCs grown in LIF or in the presence of RA for 4 d. The 3C PCR signals were calculated relative to those detected in $Satb2^{wt}$ ESCs after normalization with internal control primers. (*B*) Schematic representation of the *Nanog* locus. Previously shown interactions and primers for the 3C assay are indicated. The restriction enzyme HindIII sites used for the 3C assay are indicated as arrows. (*C*) 3C assays to assess interactions of the SATB-binding sites (SATB-BS) with the enhancer, promoter, and the 12-kb downstream region of *Nanog* locus in ESCs as described in *A*. (*D*) Global Pearson correlation clustering of HiC experiments. (*E*) Genome-wide interaction heat maps of LIF-cultured $Satb2^{wt}$ (*left*), RA-treated $Satb2^{wt}$ (*middle*), and RA-treated $Satb2^{K\rightarrow R}$ ESCs (*right*) on the intersection of all significant interactions and corresponding SATB2 ChIP-seq peaks (see Fig. 6A). Chromosome numbers are indicated. (*F*) Interaction heat maps of LIF-cultured $Satb2^{wt}$ (*left*), RA-treated $Satb2^{wt}$ (*middle*), and RA-treated $Satb2^{K\rightarrow R}$ (*right*) ESCs on the intersection of all significant interactions and corresponding SATB2 ChIP-seq peaks on chromosome 6, where *Nanog* is located. (*G*) SeqMonk browser screenshots of HiC interaction maps at the *Nanog* locus in $Satb2^{wt}$ ESCs in LIF condition (*top*), $Satb2^{wt}$ ESCs in RA d4 condition (*middle*), and $Satb2^{K\rightarrow R}$ ESCs in RA d4 condition (*bottom*). Interaction distance densities are represented as a data zoom level.

cluster) (Fig. 6B; Supplemental Table S4). In the RA-specific cluster, the peak intensities of $SATB2^{K\rightarrow R}$-bound sites were decreased relative to those of $SATB2^{wt}$ occupancy (Fig. 6B). A similar pattern of SATB2 occupancy was also detected in RA-treated $Zfp451^{-/-}$ ESCs (Supplemental Fig. S6C).

De novo motif analysis of SATB2-occupied sites in the LIF-specific cluster identified enrichment for SATB1-binding motifs in a tandem arrangement (Fig. 6C,D). In the RA-increased cluster, we detected an enrichment for SATB2-binding sites in a palindromic arrangement (Fig. 6C,D). SATB proteins recognize a 5′-ATTA core motif, but they vary in their preference of flanking nucleotides (Nakagomi et al. 1994; Yamasaki and Yamasaki 2016). Co-occurrence analysis of transcription factor motifs in a region ±100 nt of the SATB2-occupied sites showed an association of the *Satb1* motif with recognition sites for OCT4, MYB, NANOG, and AP1 in the LIF-specific cluster and an association of the *Satb2* motif with additional binding sites for CTCF, FOXO1, SMAD, and NeuroD1 in the RA-specific cluster (Supplemental Fig. S6D).

Since SATB1 and SATB2 have been found to form homo- and heterotetramers (Zheng et al. 2017), we also examined SATB1 binding in LIF- and RA-cultured $Satb2^{wt}$ and $Satb2^{K\rightarrow R}$ ESCs (Fig. 6E). This analysis identified 370 and 234 SATB1-specific peaks in LIF-cultured and RA-treated $Satb2^{wt}$ cells, respectively (Supplemental Fig. S6E). By overlapping the SATB1 peaks with SATB2 peaks, we found that 46% of LIF-specific SATB2 peaks coincide with SATB1 peaks, whereas only 8% of RA-specific SATB2 peaks overlap with SATB1 occupancy (Supplemental Fig. S6E). We further examined whether the co-occupancy of SATB1 and SATB2 changes during differentiation by probing the union of LIF- and RA-cultured

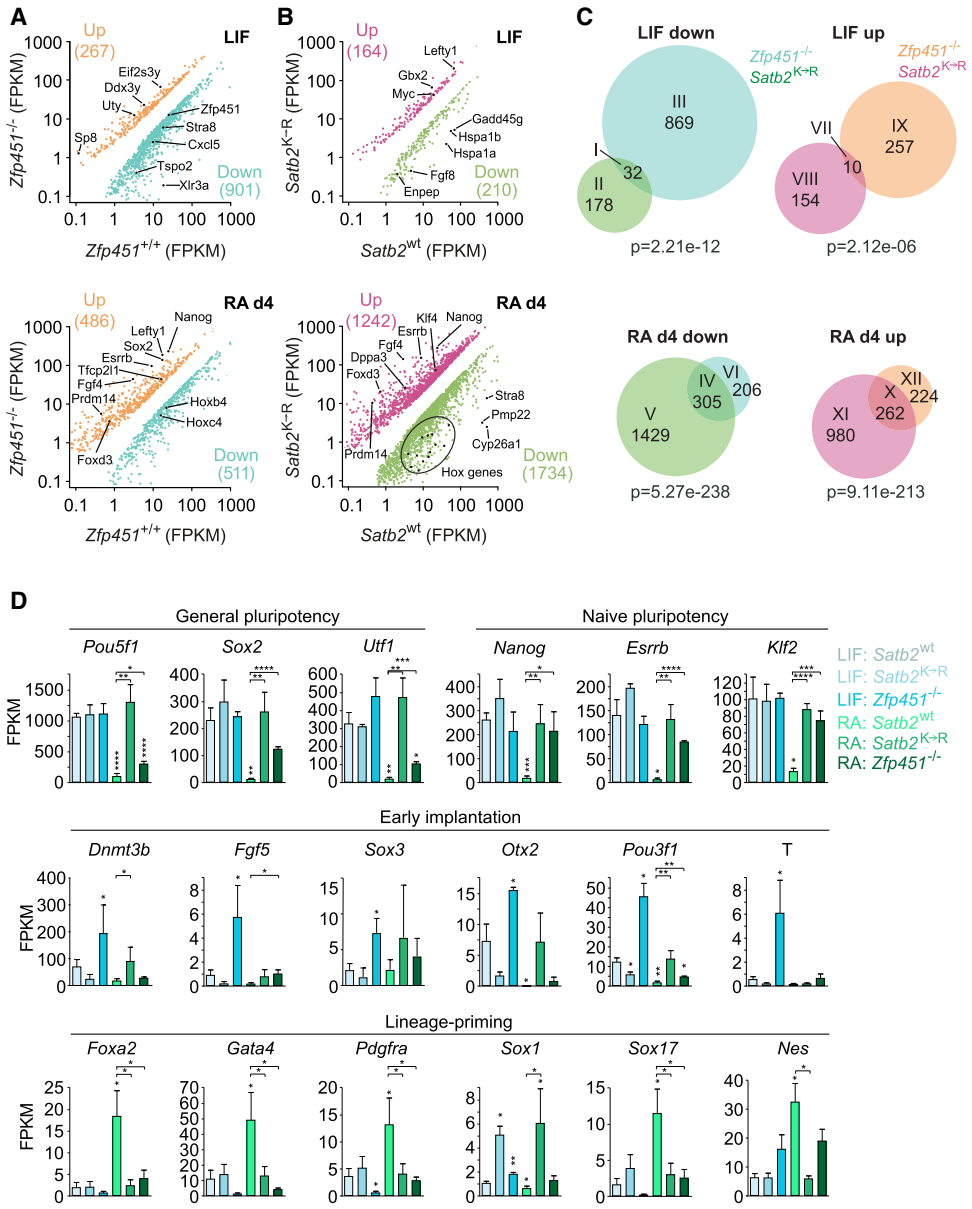

Figure 5. Impaired down-regulation of pluripotency genes in RA-treated *Satb2*$^{K\rightarrow R}$ and *Zfp451*$^{-/-}$ mESCs. (*A*,*B*) Scatter plots of normalized RNA-seq reads count (FPKM) of genes differentially expressed in *Zfp451*$^{-/-}$ ESCs (*A*) and in *Satb2*$^{K\rightarrow R}$ ESCs (*B*) relative to *Zfp451*$^{+/+}$ and *Satb2*^{wt} ESCs, respectively. Cells were cultured in LIF (*top*) or treated with RA for 4 d (*bottom*). (FPKM) Fragments per kilobase of transcript per million. (*C*) Overlap of *Zfp451*$^{-/-}$ and *Satb2*$^{K\rightarrow R}$ RNA-seq data. Venn diagrams showing common and distinct dysregulated genes in *Zfp451*$^{-/-}$ and *Satb2*$^{K\rightarrow R}$ ESCs cultured in LIF (*top*) or RA (*bottom*). The numbers of genes up- or down-regulated relative to wild-type ESCs are indicated. Roman numbers represent individual gene sets. (*D*) Barplots showing normalized FPKM quantification for representative general and naïve pluripotency genes (*top*), early implantation genes (*middle*), and lineage-priming genes (*bottom*) in *Satb2*^{wt}, *Satb2*$^{K\rightarrow R}$, *Zfp451*$^{+/+}$, and *Zfp451*$^{-/-}$ ESCs grown in LIF or RA for 4 d. Triplicate data are represented as mean ± SD. Paired *t*-tests were carried out relative to LIF-cultured *Satb2*^{wt} cells. Significance is as follows: (*) $P < 0.05$, (**) $P < 0.01$, (***) $P < 0.001$, (****) $P < 0.0001$. For analysis, *Satb2*^{wt} clones B6 ($n = 1$) and C1 ($n = 2$); *Satb2*$^{K\rightarrow R}$ clones B4, B7, and G3; *Zfp451*$^{+/+}$ clone 14 ($n = 3$); and *Zfp451*$^{-/-}$ clones 4, 7, and 10 were used.

SATB2^{wt} peaks for SATB1 signals. We clustered these regions by the presence or absence of SATB1 peaks in RA-cultured *Satb2*^{wt} ESCs (Fig. 6E). This analysis indicated that SATB1/SATB2 co-occupancy at a specific set of sites was not altered in LIF- and RA-cultured *Satb2*^{wt} and *Satb2*$^{K\rightarrow R}$ ESCs, but it also showed that the marked gain of SATB2 occupancy in RA-treated *Satb2*^{wt} cells does not involve a co-occupancy with SATB1 (Fig. 6E,F).

By using publicly available ATAC-seq data of LIF-cultured and RA-treated wild-type ESCs (Rhee et al. 2016; Wu et al. 2016), we observed that SATB1/SATB2 co-occupied regions do not coincide with open chromatin,

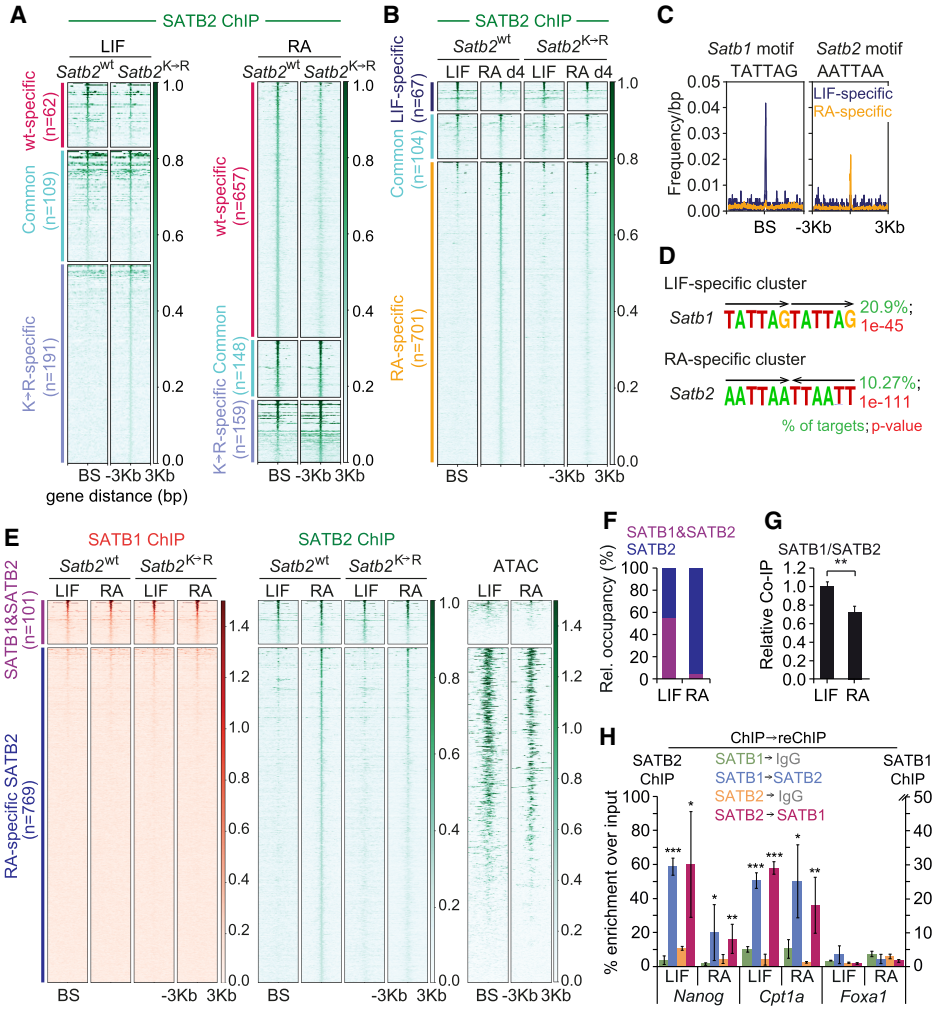

Figure 6. SUMOylation alters SATB2 occupancy in RA-treated ESCs. (*A*) Analysis of SATB2 occupancy in *Satb2*^{wt} versus *Satb2*$^{K\rightarrow R}$ ESCs cultured with LIF (*left*) or RA (*right*) for 4 d. ChIP-seq signals were retrieved on the unions of SATB2^{wt} and SATB2$^{K\rightarrow R}$ peaks in either the LIF or RA condition. Heat map of SATB2 ChIP-seq reads ± 3 kb around SATB2-binding sites (BS) are shown. The peaks were clustered as wt-specific, common, and K → R-specific. (*B*) Analysis of SATB2 occupancy in *Satb2*^{wt} and *Satb2*$^{K\rightarrow R}$ ESCs as in *A* but with ChIP-seq signals retrieved on the union of SATB2^{wt} peaks in LIF and RA conditions. The peaks were clustered as LIF- specific, common, and RA-specific in terms of their relative intensity between LIF and RA conditions in *Satb2*^{wt} cells. (*C*) Average motif frequency profiles of SATB1 (5′-TATTAG) and SATB2 (5′-AATTAA-3′) motifs in 3 kb around LIF-specifc and RA-specific SATB2 peaks. (*D*) SATB motif analysis of LIF-specific and RA-specific clusters of SATB2-occupied sites. (*E*) Heat maps of SATB1 ChIP-seq, SATB2 ChIP-seq, and ATAC-seq signals from *Satb2*^{wt} and *Satb2*$^{K\rightarrow R}$ cells cultured with LIF or with RA for d4. SATB1 ChIP-seq signals were retrieved on the union of SATB2^{wt} peaks in RA and LIF conditions. SATB2 peaks were clustered according to the presence or absence of SATB1 co-occupancy (SATB1& SATB2 occupancy or RA-specific SATB2 occupancy). (*F*) Quantification of the percentages of SATB1&SATB2- and SATB2-binding events in the LIF-specific cluster and RA-specific cluster from *B*. (*G*) LC-MS-based quantification of SATB2/SATB1 coimmunoprecipitations in pluripotent (LIF) and differentiating (RA) ESCs. Relative enrichment of endogenous SATB1 in anti-SATB2 immunoprecipitations is represented as the ratio of $\log_2$-transformed normalized summed peptide intensities (iBAQ values). Differences in heteromer formation are shown as mean ± SD (triplicate data) and with the statistical significance. Welch's *t*-test, (**) $P < 0.01$. (*H*) qRT-PCR of SATB1 or SATB2 ChIP followed by sequential ChIP (re-ChIP) of the complementary protein or control IgG. The scale for the SATB1 ChIP was increased by a factor of two to compensate for the weaker SATB1 ChIP signals. Bars show the relative enrichment over input ± SD. Paired *t*-tests were carried out relative to IgG of each re-ChIP experiment. Significance values are as follows: (*) $P < 0.05$, (**) $P < 0.01$, (***) $P < 0.001$. Experiments are representative of two independent experiments, using *Satb2*^{wt} clone C1 ($n = 2$) and *Satb2*$^{K\rightarrow R}$ clones B4 and B7.

whereas the RA-specific SATB2 regions are located in regions already accessible in LIF conditions (Fig. 6E). These data suggest that the binding of SATB2 to RA-specific sites is not due to a gain of chromatin accessibility in RA-treated cells.

To address the question of whether the co-occupancy of SATB1 and SATB2 at a specific set of sites may be accounted for by heteromer formation, we performed two sets of experiments. First, we immunoprecipitated endogenous SATB2 from lysates of LIF-cultured and RA-treated

wild-type ESCs and assessed the relative abundance of SATB2 and coimmunoprecipitated SATB1 peptides by quantitative mass spectrometry. This analysis indicated that the relative enrichment of coimmunoprecipitated SATB1 peptides was reduced in lysates of RA-treated cells (Fig. 6G). Coimmunoprecipitations of overexpressed SATB1 with either SATB2 or SUMO2-SATB2 indicated that SUMOylation of SATB2 does not affect the interaction with SATB1 (data not shown). Therefore, the reduced enrichment of SATB1/SATB2 coimmunoprecipitated peptides in RA-treated ESCs is likely due to the marked increase in SATB2 protein levels. Second, sequential ChIP (re-ChIP) analyses detected SÁTB1/SATB2 co-occupancy at *Nanog* (LIF-specific cluster) (Fig. 6B) and *Cpt1a* (common cluster) in both LIF-cultured and RA-treated ESCs, suggesting that co-occupancy occurs in the same cell and is probably not due to distinct binding in a heterogeneous cell population (Fig. 6H). In contrast, no co-occupancy was detected at the *Foxa1* locus (RA-specific cluster). Taken together, these data reveal a dynamic distribution of SATB2 occupancy during RA-induced differentiation. In pluripotent LIF-cultured ESCs, SATB2 binds target sites predominantly in association with SATB1, whereas in RA-treated ESCs, the vast majority of sites gain SATB2 occupancy in the absence of SATB1 cobinding.

To identify direct target genes of SATB2 that also change gene expression depending on the SATB2 SUMOylation status, we interrogated the SATB2 ChIP-seq data sets with the corresponding RNA-seq data sets. In LIF cultures, SATB2 binding was detected at relatively few genes that were dysregulated in $Satb2^{K\rightarrow R}$ versus $Satb2^{wt}$ cells, whereas in RA-treated cells, 155 dysregulated genes were identified as direct SATB2 targets (Supplemental Fig. S6F; Supplemental Tables S5, S6). The biological functions of these target genes were linked to differentiation, metabolism, self-renewal, and pluripotency. In $Satb2^{K\rightarrow R}$ mutant cells, SATB2 binding was detected at genes irrespective of an up-regulation or down-regulation. In $Satb2^{wt}$ cells, RA-specific gain of SATB2 occupancy was found at genes encoding regulators of ES cell differentiation, including FOXA1, a repressor of *Nanog* (Chen et al. 2014); the endoderm marker GATA4; and multiple chromatin regulators, such as APOBEC2, SETDB1, SMARCAD1, and CHD9 (Supplemental Fig. S6F). Thus, a specific set of SATB2-bound genes that are regulated during ESC differentiation depend on the SUMOylation of SATB2.

SATB2 SUMOylation promotes the interaction with the LSD1/CoREST complex

We then investigated the potential mechanism by which SUMOylation of SATB2 regulates gene expression upon RA-induced differentiation. SUMO2 modification of transcriptional regulators can lead to the recruitment of the LSD1/CoREST/HDAC1 corepressor complex via a direct interaction between SUMO2 and the SUMO-interacting motif (SIM) of CoRest (Ouyang et al. 2009). Coimmunoprecipitation experiments of endogenous SATB2 indicated that LSD1 and CoREST interact with SATB2 specifically upon RA-induced differentiation and only in the presence of SUMO-modified SATB2 (Fig. 7A). In contrast, an association of HDAC1 with SATB2 was detected in both pluripotent and differentiated cells independently of SUMOylation. Moreover, we did not detect interactions with HDAC2 or Mi-2β, which cooperate with LSD1 in the context of the NuRD complex (Whyte et al. 2012). The dependence of the LSD1-SATB2 interaction on SATB2 SUMOylation was also verified by immunoprecipitation after overexpressing the covalent SUMO2-SATB2 fusion (Fig. 7B).

To examine which SATB2 direct targets are also bound by LSD1, we performed LSD1 ChIP-seq with LIF- and RA-treated $Satb2^{wt}$ and $Satb2^{K\rightarrow R}$ ESCs and overlapped the data sets with the SATB2 ChIP-seq data. We identified a cluster of 154 SATB2-occupied sites that showed LSD1 binding only in RA-treated $Satb2^{wt}$ cells (Fig. 7C,D). Gene-specific analysis confirmed the SATB2-dependent recruitment of LSD1 at the *Nanog*, *Foxd3*, *Apobec*, and *Foxa1* loci specifically in RA-treated $Satb2^{wt}$ but not $SATB2^{K\rightarrow R}$ cells (Fig. 7E,F; Supplemental Fig. S7A). On the SATB-binding sites of the *Nanog* and *Foxd3* pluripotency genes, we noted diminished SATB2 peak signals in RA-treated ESCs. The reduced SATB2 peak signals could reflect an impaired ChIP efficiency of SUMOylated SATB2 rather than a reduced occupancy at LIF-specific sites. This possibility would not significantly affect our results and conclusions, and it would imply an even more pronounced binding of SUMOylated $SATB2^{wt}$ relative to $SATB2^{K\rightarrow R}$ at RA-specific sites in RA-treated cells (see Fig. 6B). On the *Apobec2*- and *Foxa1*- associated sites, the binding of $SATB2^{K\rightarrow R}$ was not significantly altered relative to that of $SATB2^{wt}$, indicating that the mutations of the SUMO acceptor sites of SATB2 affects LSD1 recruitment but not chromatin binding of $SATB2^{wt}$ (Supplemental Fig. S7A). GSEA analysis revealed a modest but significant enrichment of LSD1 recruitment at genes down-regulated in RA-treated $Satb2^{wt}$ versus $Satb2^{K\rightarrow R}$ ESCs (data not shown). Thus, the SUMOylation of SATB2 correlates with the recruitment of the LSD1/CoREST complex to specific gene loci and may thereby induce changes of gene expression (Supplemental Fig. S7B).

Discussion

Changes of gene expression during differentiation of stem cells are predominantly governed by stepwise alterations of transcription factor repertoires and regulatory networks (Hackett and Surani 2014; Li and Belmonte 2017). However, the initial response to differentiation cues often involves the rapid repurposing of transcription factors by post-translational modifications that alter transcriptional responses and/or target gene recognition. Here, we show that *Satb2* gene inactivation in LIF-cultured cells leads to impaired NANOG expression and destabilization of the pluripotent state, consistent with a pluripotency-promoting function of SATB2. Upon induction of differentiation, however, the interaction of SATB2 with the E3 ligase

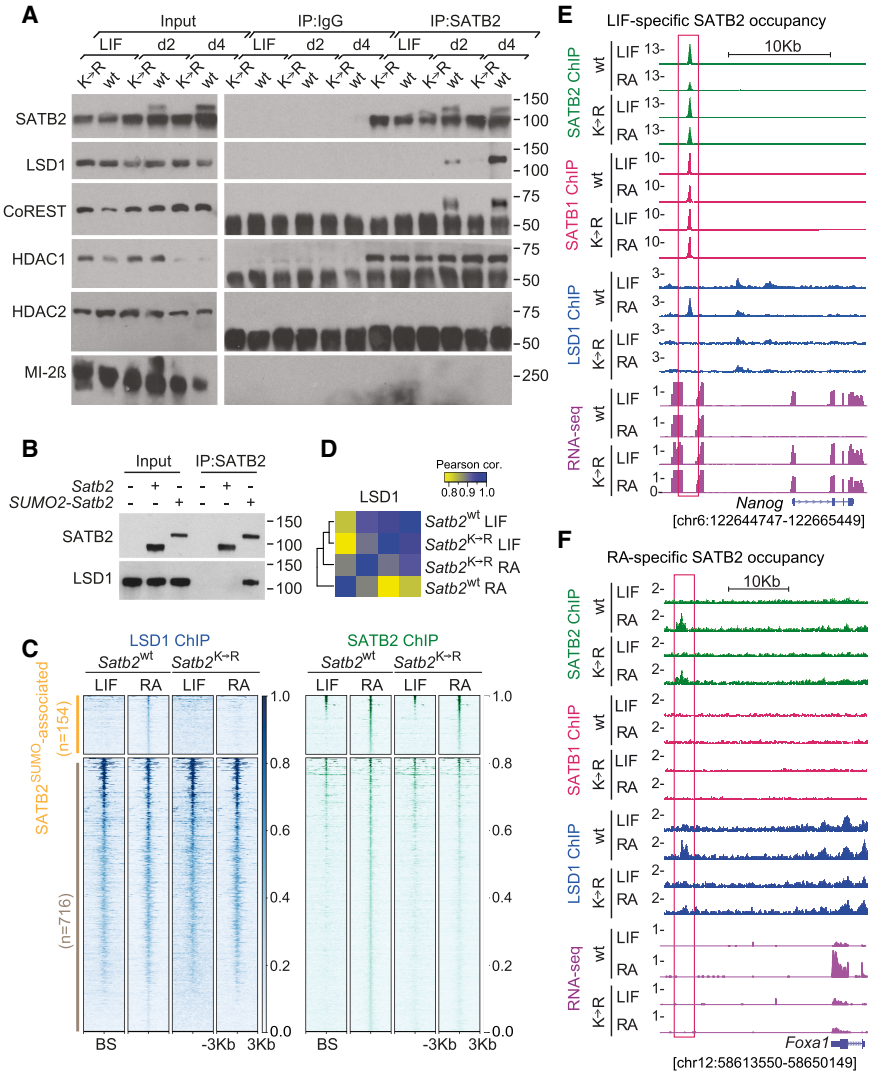

Figure 7. SUMOylation promotes the interaction of SATB2 with the LSD1/CoREST complex. (*A*) Coimmunoprecipitation of SATB2 to detect interaction with LSD1, CoREST, HDAC1, HDAC2, and Mi-2B in *Satb2*^{wt} (wt) and *Satb2*$^{K\rightarrow R}$ (K→R) ESCs, cultured with LIF or with RA for 2 d and 4 d. (*B*) Coimmunoprecipitation of LSD1 with overexpressed SATB2 and SUMO-SATB2 under LIF conditions. SUMO-SATB2 but not SATB2 interacts with LSD1. (*C*) Heat maps of LSD1 and SATB2 ChIP-seq analysis of LIF-cultured and RA-treated *Satb2*^{wt} and *Satb2*$^{K\rightarrow R}$ ESCs. The ChIP-seq signals were retrieved on the union of SATB2^{wt} peaks in RA and LIF culture conditions. The SATB2 signals were clustered according to the enrichment of LSD1 signals specifically in RA-treated *Satb2*^{wt} cells (SATB2^{SUMO}-associated and -independent clusters). (*D*) Heat map showing a correlation clustering of LSD1 signals in *Satb2*^{wt} and *Satb2*$^{K\rightarrow R}$ ESCs in LIF or RA conditions, on the union of all LSD1 peaks. (*E*,*F*) Screenshots of normalized SATB2, SATB1, and LSD1 ChIP-seq signals and RNA-seq signals in the *Nanog* locus (*E*) and the *Foxa1* locus (*F*). Red boxes highlight sites of SATB occupancy. Experiments are representative of two independent experiments, using *Satb2*^{wt} clone C1 ($n = 2$) and *Satb2*$^{K\rightarrow R}$ clones B4 and B7.

ZFP451 results in SUMO2 modification of SATB2, down-regulation of pluripotency genes, and the recruitment of the LSD1/CoREST complex to a specific set of SATB2-bound sites. SUMOylation also enables SATB2 to bind differentiation-associated genes, suggesting that this post-translational modification may allow for a repurposing of SATB2 function during the transition of pluripotent to differentiating ESCs.

Both *Satb2*$^{K\rightarrow R}$ and *Zfp451*$^{-/-}$ ESCs show an impaired differentiation potential that can be overcome by the forced expression of SUMO-SATB2 protein. Notably, both mutant ESCs can be converted to epiblast stem cells by the treatment with FGF and Activin A, suggesting that the cells can exit from the state of naïve pluripotency and acquire the state of primed pluripotency. Thus, the impaired differentiation may affect lineage commitment, which involves the down-regulation of naïve pluripotency genes and the expression of lineage markers. Our combined ChIP-seq and RNA-seq analysis identified SATB2-bound genes that are commonly dysregulated in RA-treated *Satb2*$^{K\rightarrow R}$ and *Zfp451*$^{-/-}$ ESCs. Both mutant cells show an up-regulation of the naïve pluripotency genes *Nanog*, *Foxd3*, *Smarcad1* and a down-regulation of the differentiation gene *Gata4*.

NANOG is a key determinant of pluripotency that rewires the regulatory network by cobinding with other pluripotency factors to many enhancers and by enhancing chromatin accessibility (Chambers et al. 2007; Heurtier et al. 2019). In addition, NANOG engages in an antagonistic network with OTX2 to confer upon LIF-cultured ESCs a responsiveness to naïve or primed pluripotency-inducing factors (Acampora et al. 2017). FOXD3 is also required for the maintenance of pluripotency and acts as a repressor that dismantles the naïve pluripotency gene expression program by decommissioning active enhancers and promoting the transition to the primed pluripotent state (Hanna et al. 2002; Krishnakumar et al. 2016; Respuela et al. 2016). SMARCAD1 enhances naïve pluripotency by binding to citrullinated histone H3R26cit, which suppresses H3K9me3-driven heterochromatin (Xiao et al. 2017). In addition, SMARCAD1 and MORC1, which are both bound by SATB2 and up-regulated in *Satb2*$^{K\rightarrow R}$ and

Zfp451$^{-/-}$ ESCs, are involved in the silencing of endogenous retroviruses (Pastor et al. 2014; Sachs et al. 2019).

In LIF-cultured *Satb2*$^{K\rightarrow R}$ cells, we observed a down-regulation of early postimplantation genes associated with the primed pluripotency state, including *Fgf5*, *Otx2*, and *Pou3f1* (Oct6), relative to wild-type cells, suggesting a role of SATB2^{K233} and/or SATB2^{K350} modifications already prior to differentiation-induced SUMO2 modification SUMOylation by ZFP451. Consistent with the lack of a detectable interaction between SATB2 and ZFP451 in LIF culture conditions, we observed virtually no common changes of gene expression in LIF-cultured *Satb2*$^{K\rightarrow R}$ and *Zfp451*$^{-/-}$ ESCs. The observed alterations of gene expression in LIF-cultured *Satb2*$^{K\rightarrow R}$ ESCs raise the possibility that these cells have acquired a state with hallmarks of both naïve and primed pluripotency that may resemble the transitional state of "formative" pluripotency (Smith 2017; Neagu et al. 2020). The primed pluripotent state, associated with epiblast stem cells, confers a reduced potential in chimeric assays (Mascetti and Pedersen 2016). Our analysis of the stem cell potential of *Satb2*$^{K\rightarrow R}$ and *Zfp451*$^{-/-}$ ESCs suggested that both mutant cells have a reduced potential to contribute to chimera formation. Thus, these cells may represent a pluripotent state with both impaired differentiation and stem cell potential.

Despite the differentiation-specific ZFP451:SATB2 interaction, we detected ZFP451 expression in pluripotent cells at an even higher level than in differentiating cells. Mass spectrometric and biochemical analysis showed that human ZNF451 is SUMOylated (Karvonen et al. 2008; Hendriks et al. 2015, 2018), raising the possibility that SUMOylation of ZFP451 during differentiation could affect its substrate interaction and enzymatic activity. Indeed, ZNF451 is itself a SUMO2 target (Eisenhardt et al. 2015), and fusion of SUMO2 to ZNF451 likely enhances its enzymatic activity (Cappadocia et al. 2015). Alternatively, the SATB2:ZFP451 interaction could be regulated by differential PTMs of SATB2 in pluripotent versus differentiating ESCs. The SUMO targeted lysine 350 of the SATB2 protein resides within a highly conserved acetylation-to-SUMOylation switch motif (ψKxEP), which is found in other transcriptional regulators such as HIC1, C/EBP, and GATA1 (Stankovic-Valentin et al. 2007; Van Rechem et al. 2010). Thus, a switch in PTM rather than de novo SUMOylation of unmodified lysines may underlie the functional repurposing of Satb2 in differentiating ESCs.

To date, the SUMO2-specific E3 ligase ZNF451 has been studied primarily during various stress conditions with a handful of substrates, including Sp100, PML, HDAC4, and MCM4 (Cappadocia et al. 2015; Eisenhardt et al. 2015; Koidl et al. 2016). Moreover, ZNF451/ZATT has been identified as a DNA repair factor that interacts with genotoxic TOP2 DNA:protein cross-links (Schellenberg et al. 2017). Although SATB2 is a functionally important target for SUMO2 modification by ZFP451 in differentiating ESCs, ZFP451 is likely to have additional and unrelated targets. *Zfp451* knockout mice are viable, but high-throughput phenotype analysis of adult homozygous mutant mice reported hypoactivity and male-specific abnormalities of skin and pancreas (International Mouse Phenotyping Consortium, http://www.mousephenotype.org; Dickinson et al. 2016) In contrast, *Satb2* knockout mice have skeletal and neuronal defects, and they die shortly after birth (Dobreva et al. 2006; Alcamo et al. 2008; Britanova et al. 2008). The perinatal viability of both *Satb2*$^{-/-}$ and *Zfp451*$^{-/-}$ mice is in contrast to the differentiation defects of the corresponding ESCs. Similar discrepancies of mutant phenotypes in cultured ES cells and mice have been described for several genes encoding RNA- and/or chromatin-modifying enzymes, such as Mettl5 (Vougiouklakis et al. 2017; Ignatova et al. 2020). Such discrepancies could be due to potential compensatory effects in vivo and/or a signaling environment in the developing embryo that overrides cell-intrinsic defects observed in cultured ES cells. Thus, the findings on the role of SATB2 SUMOylation for embryonic stem cell differentiation may be limited to in vitro cultured cells.

Our ChIP-seq data suggest that RA treatment of wild-type ESCs results in a gain of SATB2 binding at many differentiation-associated genes. Altered binding to specific subsets of target sites has also been observed upon SUMOylation of nuclear hormone receptors and GATA1 (Lee et al. 2009; Paakinaho et al. 2014; Sutinen et al. 2014). The differentiation-specific sites of SATB2 occupancy are predominantly associated with lineage-specific genes, and the *Satb2*$^{K\rightarrow R}$ mutation affects both activation and repression. In RA-treated *Satb2*$^{K\rightarrow R}$ ESCs, many dysregulated genes lose the recruitment of the LSD1/CoREST complex, which has been shown to confer gene activation and repression, dependent on the composition of the complex (Wang et al. 2007). Moreover, the LSD1/CoREST complex is required for embryonic development and for the efficient repression of pluripotency genes during neural differentiation (Qureshi et al. 2010; Adamo et al. 2011). Thus, SUMOylation of SATB2 correlates with recruitment of the LSD1/CoREST complex, which may help to diversify the function of Satb2 in ESCs. SATB1/SATB2 heteromers may facilitate binding at low SATB2 concentration in LIF-cultured ESCs independently of accessible chromatin domains. Recent analysis of SATB1 binding indicated that SATB1 binds inaccessible chromatin domains with a preference of multiple consensus motifs (Ghosh et al. 2019). In conditions of differentiation, the marked increase in SATB2 level and SUMOylation may both allow for binding to a new set of sites independently of SATB1.

Our analysis shows that SUMOylation of SATB2 is necessary but not sufficient for the differentiation of ESCs and the down-regulation of pluripotency genes. The forced expression of a SUMO-Satb2 fusion protein can rescue, at least in part, the differentiation defect of *Satb2*$^{K\rightarrow R}$ ESCs only upon RA treatment, suggesting that differentiation-specific interaction partners or additional post-translational modifications may cooperate with SUMO-SATB2 to shift the balance from pluripotency to differentiation. According to this view, SUMOylation of SATB2 may destabilize the pluripotency gene regulatory network and allow differentiation cues to collapse this network

and to initiate lineage-specific programs. Considering that SUMO function has recently been implicated in the maintenance of cell identity (Borkent et al. 2016; Cossec et al. 2018; Theurillat et al. 2020), ZFP451-mediated SUMO2 modification of SATB2 may also contribute to stabilizing the differentiated state of somatic cells.

Materials and methods

Cell culture

All mouse embryonic stem cell lines were cultured and passaged on irradiated mouse embryonic fibroblasts in ES cell medium containing 15% PANSera ES serum (PAN Biotech) and 1000 U/mL ESGRO LIF (Millipore) as well as 1× sodium pyruvate (GIBCO), 1× penicillin/streptomycin/glutamine (GIBCO), 1× nonessential amino acids (GIBCO), 0.1 mM β-mercaptoethanol (Sigma), and DMEM high glucose (ThermoFisher). For differentiation experiments and RNA/DNA/protein extractions, ESCs were cultured on dishes covered with 0.1% gelatin, except $Satb2^{\Delta/\Delta}$ ESCs, which were cultured on dishes covered with fibronectin.

mESC differentiation

For differentiation of ESCs to epiblast stem cells, ectoderm, endoderm, and random progenitors, mESCs were initially plated on 0.1% gelatin-covered dishes in ES cell media. Twenty-four hours later, the media was switched to the appropriate differentiation medium. Epiblast differentiation was induced with epiblast medium: 50% IMDM (Gibco; supplemented with 2 mM of L-glutamine), 50% Ham's F-12 nutrient mix (Gibco; supplemented with 2 mM L-glutamine), 5 mg/mL BSA, 1%, 450 µM 1-thioglycerol, 7 µg/mL recombinant insulin (Thermo), 15 µg/mL transferrin (Sigma; supplemented freshly with 12 µg/mL of FGF2[R&D]), and 20 µg/mL Activin A (R&D). Ectoderm precursors were generated with ES cell medium containing serum + 5 µM retinoic acid (Sigma) or neuroectoderm medium: 44% DMEM/F12 (Gibco), 44% neurobasal (Gibco), 1× N2 and 1× B27 supplements (Gibco), 20 ng/mL Fgf2 (R&D), 400 ng/mL Sonic Hedgehog (SHH; R&D), 100 ng/mL Fgf8 (Gibco), and 1× penicillin/streptomycin (Gibco). Endoderm differentiation was induced with endoderm medium: 74% IMDM (Gibco), 25% DMEM/F12 (Gibco), 1× N2 and 1× B27 supplements (Gibco), 2 mM l-glutamine (PAN), 0.05% BSA (Sigma), 0.5 mM ascorbic acid (StemCell), 0.45 mM β-mercaptoethanol (Sigma), 1× nonessential amino acids (Gibco), 1× penicillin/streptomycin (Gibco), and 50 ng/mL Activin A (R&D). Random differentiation was achieved by culture in ES cell media without LIF. For mesoderm differentiation, ES cells were plated on type IV collagen-coated six-well cluster dishes (Biocoat; Becton-Dickinson) and incubated in α-MEM (Thermofisher) supplemented with 10% PANSera ES (PAN Biotech), 1× penicillin/streptomycin (Gibco), and 0.45 mM β-mercaptoethanol (Sigma).

CRISPR/Cas9 editing of mESCs

CRISPR guide RNAs (gRNAs) were designed using the online tool from the Massachusetts Institute of Technology (http://crispr.mit.edu). gRNAs were cloned into pCas9 (BB) 2A-GFP (pX458; Addgene 48138). A minimum of three gRNAs were screened for each locus, and their efficiency was determined using the T7 endonuclease assay as described before (Ran et al. 2013). K → R mutations in the Sumo acceptor sites 233 and 350 or the Satb2 protein were generated by inserting subsequently individual mutations. A single-stranded donor oligonucleotide was used for K350R, and double-stranded donor plasmid was used for K233R. The donor oligonucleotide or donor plasmid was transiently cotransfected with their respective gRNA (K233R: 5′-ACACTGCACA CAGTCCATAC-3′; K350R: 5′-ACAGAGGAGTTTGTTGGC TC-3′). Successful mutation was determined by PCR followed by restriction digestion of the amplicon. Positive clones were confirmed by Sanger DNA sequencing (K233: Fwd 5′-ATTTCGTTT GTAGAGGAGTCATAGC-3′, K233: Rev 5′-CTAATGGATTTT GGCTTTTAT-3′, K350: Fwd 5′-ACTGACTCACTTTTGTTTT GGG-3′, and K350: Rev 5′-GCGGTTGAATGCCACTCTTG-3′). For the C-terminal tagging of the Satb2 protein, a gRNA (5′-TATCTC TGGTCGGTTTCGGC-3′) and a donor plasmid containing the 3xTy1 tag were transfected as described above. Positive colonies were screened with the primers Ty1-Fwd (5′-CCTCTATCCCGACCAGGAAGC-3′) and Ty1-Rev (5′-AGTGT CTTTGCCAAG GTGACG-3′).

Generation of Zfp451 knockdown ES cell lines

Knockdown of the *Zfp451* gene in mouse ESCs was achieved with a retroviral vector. Virus was produced in platE cells transfected with 17 µg of the pQCXIN vector (Clontech) containing a shRNA directed against the isoforms 1 and 2 of the *Zfp451* gene (target sequence: 5′-TTTCATAGTGGGCATAGATA-3′).

Generation of EpiSCs

$Satb2^{wt}$, $Satb2^{K\rightarrow R}$, and $Zfp451^{-/-}$ mESC cell lines were grown for 5 d in a normal mES cell medium containing FGF2 and Activin A. Complete differentiation into epiblast stem cells was further confirmed by checking morphology, quantitative RT-PCR, and Western blot analysis of epiblast stem cell-specific markers.

Generation of chimeric embryos

$Satb2^{wt}$, $Satb2^{K\rightarrow R}$, and $Zfp451^{-/-}$ mESC cell lines stably expressing tdTomato were generated using a pCAH-NLS-tdTomato plasmid vector. Reporter mESC cell lines were microinjected into B6(C)Rj-Tyrc/c E3.5 mouse preimplantation embryos (blastocysts) and transferred to pseudopregnant females (licenses Az. 35-9185.82/I-17/01 and Az. 35-9185.82/I-17/03). Embryos were collected at E10.5. All mice were kept in the animal facility of the Max Planck Institute of Immunobiology and Epigenetics under specific pathogen-free conditions. All animal experiments were performed in accordance with the relevant guidelines and regulations, approved by the review committee of the Max Planck Institute of Immunobiology and Epigenetics and the Regierungspräsidium Freiburg, Germany (license Az.35-9185.81/G-18/117).

Staining of embryos

E10.5 embryos were fixed in 4% PFA and permeabilized with 0.5% Triton X-100 followed by blocking with 3% BSA overnight. Blocked embryos were stained with anti-tdTomato antibody followed by Alexa Fluor 555 antirabbit IgG secondary antibody staining. Microscopic images were acquired with a LSM 880 AxioObserver (Zeiss): objective: plan-apochromat: 5×/0.16 M27, and light source: DPSS 561 nm. Tiles images were acquired every 4 µm of the focal plane. Images were then reconstituted using the Fiji software (ImageJ, version 2.0.0-rc-59/1.51 k), using the automated stitching plugging. For each embryo, a volume of 200 µm (50 stacks) was used to create 2D images (hyperstacks) using maximum intensity projection.

Detection of endogenous SUMOylation

To detect endogenous SUMO-Satb2 conjugates in ES cells, the protocol from Becker et al. (2013) was followed to detail. SUMO hybridomas SUMO1 21C7 and SUMO2 8A2 were developed by M. Matunis and obtained from the Developmental Studies Hybridoma Bank, created by the National Institute of Child Health and Human Development of the National Institutes of Health and maintained at Department of Biology, The University of Iowa (Becker et al. 2013; http://dshb.biology.uiowa.edu). The antibodies were cross-linked to protein G-agarose (Roche). SUMO conjugates were eluted with buffer containing epitope-containing peptides (for SUMO1 21C7, VPMNSLRFLFE; for SUMO2 8A2, IRFRFDGQPI).

In vitro SUMOylation assay

Recombinant SATB2^{wt}, SATB2$^{K\rightarrow R}$, and ZFP451-N (6xHis-MBP-ZNF451 amino acids 2–246) (Eisenhardt et al. 2015) were purified and used at equimolar concentrations. In vitro SUMO modification assays were performed using an in vitro SUMOylation kit from Enzo Life Sciences (BML-UW8955), according to the manufacturer's instructions. Reactions were incubated at 37°C and were stopped by 1:1 dilution with 2× reducing sample buffer with DTT. The samples were further analyzed by Western blotting using anti-Satb2 antibody.

RNA isolation and qRT-PCR

RNA was purified using Trizol (Life Technologies) according to the manufactureŕs instructions. For RNA-seq, the RNA was further cleaned with the RNeasy mini kit (Qiagen). RNA (0.1–1 µg) was used to prepare cDNA with the SuperScript II reverse transcriptase (Invitrogen) system and analyzed by quantitative RT-PCR using the Fast SYBR Green master mix (Applied Biosystems). Primers are listed in the Supplemental Material.

RNA-seq library preparation, sequencing, and data analysis

Libraries were prepared from 1 µg of purified total RNA using the TruSeq stranded mRNA sample preparation kit (Illumina) and quantified with a Qubit fluorometer (Thermo). Uniquely indexed libraries were pooled in equimolar ratios and sequenced on an Illumina NextSeq500. RNA-seq data were mapped to the mouse reference genome (mm9) using Tophat (v2.0.14) (Cossec et al. 2018). The mapped reads were further assembled using Cufflinks (v2.2.1), and the expression level of the reference genes (UCSC, mm9) was determined by Cuffquant. The two biological replicates of each condition were normalized, and the differential gene expression between the conditions was calculated using Cufflinks tools (Trapnell et al. 2012). The gene sets were further filtered with the q-value cutoff < 0.05 and twofold up-regulation or down-regulation relative to the wild-type cells. Further details are available in the Supplemental Material.

Immunoblot analyses

A full list of antibodies used in the immunoblot analyses is in the Supplemental Material.

ChIP protocol and library preparation

The ChIP protocol for pluripotent and differentiating ES cells was adapted from Lee et al. (2006) and optimized as follows. The cells were cross-linked with 1% methanol-free formaldehyde (Thermo/Pierce) for 10 min. Glycine solution was added to a final concentration of 125 mM to stop the cross-linking. The cells were sonicated in E220 Ultrasonicator (Covaris) with following settings: 140 peak incidence, 5 duty factor, 200 cycles/burst, and 1200 sec. Ten micrograms of antibody (see the Supplemental Material) and blocked (0.5% BSA in PBS) GammaBind G Sepharose beads was added to the precleared lysate for the ChIP. The input and eluates were purified using the QIAquick PCR purification kit (Qiagen). Full details are in the Supplemental Material.

ChIP-seq data processing

Reads were aligned in paired-end mode to the mm9 genome using bowtie2 v2.2.8 (Langmead and Salzberg 2012). Peak calling and read coverage generation were performed using macs2 v2.1.2 (Zhang et al. 2008). To compute differentially bound regions, peak summits were merged using bedtools mergev2.19.0 (Quinlan and Hall 2010) with -d 400 as a parameter, and read coverages were retrieved over merged peak summits as count matrices using Homer annotatePeaks v4.7 (Heinz et al. 2010). Differentially bound regions were called as previously described (Cauchy et al. 2016) as having an absolute $\log_2$ fold change ≥1 on the union of wt LIF and RA Satb2 peaks. Where applicable, differential and shared regions were further split by Satb1 (d4 wt) overlap or LSD1 peak gain (d4 wt). Heat maps and average profiles were generated using deeptools v2.4.2 (Ramírez et al. 2014). LSD1 ChIP-seq clustering was performed on the union of all LSD1 peaks in all conditions, ±200 bp from peak centers, using the R gplots heatmap.2 function. Further details are in the Supplemental Material.

Motif discovery

Motif discovery was performed using Homer with default parameters. Motif average profiles were obtained via Homer annotatePeaks v4.7 and deeptools v2.4.2. Full details are in the Supplemental Material.

HiC assay

HiC was performed was performed according to the in-situ HiC protocol with slight modifications as previously described (Rao et al. 2014; Mumbach et al. 2016). Briefly, cells were cross-linked for 10 min at room temperature in 1% formaldehyde and quenched with 125 mM glycine for 5 min at room temperature. HiC reactions were performed in 10^7 cross-linked cells using 50 µL of 10× NEB buffer 2 and 375 U of MboI restriction enzyme (NEB R0147). Samples were sonicated in a Covaris militube using a Covaris E220 sonicator (fill level: 10, duty cycle: 5, PIP: 140, cycles/burst: 200, and time: 4 min). Biotin pull-down was carried out using 50 ng of chromatin via magnetic separation. For PCR and post-PCR size selection, beads were resuspended in 50 µL of PCR master mix (2× Phusion HF,12.5 µM Nextera Ad1.1 [universal], 12.5 µM Nextera Ad2.x [barcoded]) with 15 cycles (15 sec at 98°C, 30 sec at 63°C, and 1 min at 72°C). Libraries were cleaned up with 1.8× and subsequently 0.6× Ampure XP beads, and finally eluted in 10 µL of water. Sequencing was carried out on an Illumina HiSeq 2500 sequencer. Full details are in the Supplemental Material.

HiC data analysis

Reads were aligned to the mm9 genome using bwa (v 0.7.16a) (Li and Durbin 2009). Corrected interaction matrices were obtained via HiCExplorer (v2.1.4) (Ramírez et al. 2018). Significant interactions were called using Homer. HiC matrix correlation

was carried out using hicCorrelate of the HiCExplorer (v2.1.4) package. Interactions were plotted using SeqMonk (v1.4.6).

3C assay

For each sample, 1 million to 2 million cells were lysed in 300 µL of lysis buffer (10 mM Tris-HCl at pH 8.0, 10 mM NaCl, 0.2% Igepal CA630 with protease inhibitors) and incubated for 20 min on ice. Cells were centrifuged 2500*g* for 5 min at 4°C, and pellets were washed once in lysis buffer. Pellets were resuspended in 50 µL of 0.5% SDS and incubated for 10 min at 65°C. Water (145 µL) and 25 µL of 10% Triton X-100 were added to the samples and incubated for 15 min at 37°C. HindIII restriction enzyme (100 U) and 25 µL of NEB Cut smart buffer were added and incubated overnight at 37°C with shaking. The next day, the enzyme was inactivated for 20 min at 65°C. The ligation reaction was carried out overnight at 16°C by adding 120 µL of NEB T4 ligase buffer with 10 mM ATP (NEB B0202), 100 µL of 10% Triton X-100, 3 µL of 50 mg/mL BSA, 720 µL of water, and 5 µL of T4 DNA ligase (NEB M0202). The day after, 50 µL of 20 mg/mL proteinase K and 120 µL of 10% SDS were added, and the samples were incubated overnight at 65°C. Last, 10 µL of 10 mg/mL RNase was added, and samples were incubated for 1 h at 37°C. Following phenol chloroform purification, the DNA was precipitated using 1.6 vol of 100% ethanol and 0.1 vol of 3 M sodium acetate. After incubation for 1 h at −80°C, samples were spun at 16000 rpm for 15 min at 4°C. Pellets were washed twice with 70% ethanol and dissolved in 100 µL of 10 mM Tris (pH 8.0). 3C ligation products were measured by quantitative PCR, and primers for the amplification of the "bait" sequence were used as an internal normalization control for each of the samples. The primers used for this study are in the Supplemental Material.

Data availability

ChIP-seq, RNA-seq and HiC data were deposited at the Gene Expression Omnibus (GEO) under the accessions GSE119989 (ChIP-seq), GSE119990 (RNA-seq), GSE153078 (HiC), and GSE119991 (SuperSeries).

Competing interest statement

The authors declare no competing interests.

Acknowledgments

We thank Sina Ruprecht and Robert Nechanitzky for their contributions to the project outline, Frauke Melchior (ZMBH, Heidelberg) for providing the protocol to enrich SUMOylated proteins prior to publication, and Jan Breucker (A.P. laboratory) for providing bead-coupled anti-SUMO antibodies for initial analysis and for advice. We thank Yutthaphong Phongbunchoo for purifying Satb2 proteins and Natalie Eisenhardt (A.P. laboratory) for advice. We extend our thanks to Liubov Chechik (R.G. laboratory) for help with Satb2$^{-/-}$ ES cell cultures, and to Ekaterina Lupar (R.G. laboratory) for FACS analysis of TdTomato stainings. We thank Gerhard Mittler (Proteomics Core Facility) and Benoit Kanzler (Transgenic Core Facility) for LC-MS analysis and embryo injections, respectively. We also thank Petra Kindle (Imaging Core Facility) for imaging of morulae. We are grateful to Stephane Vincent (IGBMC, Strasbourg) for advice in chimera analysis, and thank Ritwick Sawarkar and Marc Stemmler for discussions, and Marika Rott for assistance with the manuscript preparation. This work was supported by funds of the Max Planck Society (MPS) and the German Research Foundation. Research in the J.J.P. laboratory is supported by the Academy of Finland. Research in the A.P. laboratory is supported by the MPS, the Wilhelm Sanders Stiftung, and a Marie Sklodowska-Curie grant of the European Union's Horizon 2020 research and innovation program.

Author contributions: G.A.U. designed and performed most experiments and wrote the manuscript. H.R. generated the CRISPR/Cas9-mediated gene-edited ESC lines and performed the Satb2 immunoprecipitations for mass spectrometry. P.C. analyzed genomics and RNA-seq data sets, wrote the manuscript, and performed the Satb2 ChiP-seq in RA-cultured Zfp$^{-/-}$ cells. S.R. analyzed RNA-seq data sets. K.B. and S.B. performed experiments, E.D. (A.P. laboratory) performed preliminary in vitro SUMOylation assays, T.C. (E.T. laboratory) conducted imaging. M.-E.T.-P. and E.T. provided advice. A.P. and J.J.P. provided unpublished information and advice. R.G. designed experiments, wrote the manuscript, and supervised the study.

References

Acampora D, Omodei D, Petrosino G, Garofalo A, Savarese M, Nigro V, Di Giovannantonio LG, Mercadante V, Simeone A. 2016. Loss of the Otx2-binding site in the nanog promoter affects the integrity of embryonic stem cell subtypes and specification of inner cell mass-derived epiblast. *Cell Rep* **15:** 2651–2664. doi:10.1016/j.celrep.2016.05.041

Acampora D, Di Giovannantonio LG, Garofalo A, Nigro V, Omodei D, Lombardi A, Zhang J, Chambers I, Simeone A. 2017. Functional antagonism between OTX2 and NANOG specifies a spectrum of heterogeneous identities in embryonic stem cells. *Stem Cell Reports* **9:** 1642–1659. doi:10.1016/j.stemcr.2017.09.019

Adamo A, Sesé B, Boue S, Castaño J, Paramonov I, Barrero MJ, Izpisua Belmonte JC. 2011. LSD1 regulates the balance between self-renewal and differentiation in human embryonic stem cells. *Nat Cell Biol* **13:** 652–659. doi:10.1038/ncb2246

Alcamo EA, Chirivella L, Dautzenberg M, Dobreva G, Fariñas I, Grosschedl R, McConnell SK. 2008. Satb2 regulates callosal projection neuron identity in the developing cerebral cortex. *Neuron* **57:** 364–377. doi:10.1016/j.neuron.2007.12.012

Apostolou E, Ferrari F, Walsh RM, Bar-Nur O, Stadtfeld M, Cheloufi S, Stuart HT, Polo JM, Ohsumi TK, Borowsky ML, et al. 2013. Genome-wide chromatin interactions of the Nanog locus in pluripotency, differentiation, and reprogramming. *Cell Stem Cell* **12:** 699–712. doi:10.1016/j.stem.2013.04.013

Becker J, Barysch SV, Karaca S, Dittner C, Hsiao HH, Berriel Diaz M, Herzig S, Urlaub H, Melchior F. 2013. Detecting endogenous SUMO targets in mammalian cells and tissues. *Nat Struct Mol Biol* **20:** 525–531. doi:10.1038/nsmb.2526

Borkent M, Bennett BD, Lackford B, Bar-Nur O, Brumbaugh J, Wang L, Du Y, Fargo DC, Apostolou E, Cheloufi S, et al. 2016. A serial shRNA screen for roadblocks to reprogramming identifies the protein modifier SUMO2. *Stem Cell Reports* **6:** 704–716. doi:10.1016/j.stemcr.2016.02.004

Britanova O, de Juan Romero C, Cheung A, Kwan KY, Schwark M, Gyorgy A, Vogel T, Akopov S, Mitkovski M, Agoston D, et al. 2008. Satb2 is a postmitotic determinant for upper-layer neuron specification in the neocortex. *Neuron* **57:** 378–392. doi:10.1016/j.neuron.2007.12.028

Cai S, Lee CC, Kohwi-Shigematsu T. 2006. SATB1 packages densely looped, transcriptionally active chromatin for coordinated expression of cytokine genes. *Nat Genet* **38:** 1278–1288. doi:10.1038/ng1913

Cappadocia L, Pichler A, Lima CD. 2015. Structural basis for catalytic activation by the human ZNF451 SUMO E3 ligase. *Nat Struct Mol Biol* **22:** 968–975. doi:10.1038/nsmb.3116

Cauchy P, Maqbool MA, Zacarias-Cabeza J, Vanhille L, Koch F, Fenouil R, Gut M, Gut I, Santana MA, Griffon A, et al. 2016. Dynamic recruitment of Ets1 to both nucleosome-occupied and -depleted enhancer regions mediates a transcriptional program switch during early T-cell differentiation. *Nucleic Acids Res* **44:** 3567–3585. doi:10.1093/nar/gkv1475

Chambers I, Colby D, Robertson M, Nichols J, Lee S, Tweedie S, Smith A. 2003. Functional expression cloning of Nanog, a pluripotency sustaining factor in embryonic stem cells. *Cell* **113:** 643–655. doi:10.1016/S0092-8674(03)00392-1

Chambers I, Silva J, Colby D, Nichols J, Nijmeijer B, Robertson M, Vrana J, Jones K, Grotewold L, Smith A. 2007. Nanog safeguards pluripotency and mediates germline development. *Nature* **450:** 1230–1234. doi:10.1038/nature06403

Chen T, He S, Zhang Z, Gao W, Yu L, Tan Y. 2014. Foxa1 contributes to the repression of Nanog expression by recruiting Grg3 during the differentiation of pluripotent P19 embryonal carcinoma cells. *Exp Cell Res* **326:** 326–335. doi:10.1016/j.yexcr.2014.04.020

Cossec JC, Theurillat I, Chica C, Búa Aguin S, Gaume X, Andrieux A, Iturbide A, Jouvion G, Li H, Bossis G, et al. 2018. SUMO safeguards somatic and pluripotent cell identities by enforcing distinct chromatin states. *Cell Stem Cell* **23:** 742–757.e8. doi:10.1016/j.stem.2018.10.001

Dickinson LA, Dickinson CD, Kohwi-Shigematsu T. 1997. An atypical homeodomain in SATB1 promotes specific recognition of the key structural element in a matrix attachment region. *J Biol Chem* **272:** 11463–11470. doi:10.1074/jbc.272.17.11463

Dickinson ME, Flenniken AM, Ji X, Teboul L, Wong MD, White JK, Meehan TF, Weninger WJ, Westerberg H, Adissu H, et al. 2016. High-throughput discovery of novel developmental phenotypes. *Nature* **537:** 508–514. doi:10.1038/nature19356

Dobreva G, Dambacher J, Grosschedl R. 2003. SUMO modification of a novel MAR-binding protein, SATB2, modulates immunoglobulin μ gene expression. *Genes Dev* **17:** 3048–3061. doi:10.1101/gad.1153003

Dobreva G, Chahrour M, Dautzenberg M, Chirivella L, Kanzler B, Fariñas I, Karsenty G, Grosschedl R. 2006. SATB2 is a multifunctional determinant of craniofacial patterning and osteoblast differentiation. *Cell* **125:** 971–986. doi:10.1016/j.cell.2006.05.012

Eisenhardt N, Chaugule VK, Koidl S, Droescher M, Dogan E, Rettich J, Sutinen P, Imanishi SY, Hofmann K, Palvimo JJ, et al. 2015. A new vertebrate SUMO enzyme family reveals insights into SUMO-chain assembly. *Nat Struct Mol Biol* **22:** 959–967. doi:10.1038/nsmb.3114

Enserink JM. 2015. Sumo and the cellular stress response. *Cell Div* **10:** 4. doi:10.1186/s13008-015-0010-1

Galande S, Dickinson LA, Mian IS, Sikorska M, Kohwi-Shigematsu T. 2001. SATB1 cleavage by caspase 6 disrupts PDZ domain-mediated dimerization, causing detachment from chromatin early in T-cell apoptosis. *Mol Cell Biol* **21:** 5591–5604. doi:10.1128/MCB.21.16.5591-5604.2001

Galande S, Purbey PK, Notani D, Kumar PP. 2007. The third dimension of gene regulation: organization of dynamic chromatin loopscape by SATB1. *Curr Opin Genet Dev* **17:** 408–414. doi:10.1016/j.gde.2007.08.003

Ghosh RP, Shi Q, Yang L, Reddick MP, Nikitina T, Zhurkin VB, Fordyce P, Stasevich TJ, Chang HY, Greenleaf WJ, et al. 2019. Satb1 integrates DNA binding site geometry and torsional stress to differentially target nucleosome-dense regions. *Nat Commun* **10:** 3221. doi:10.1038/s41467-019-11118-8

Goolam M, Zernicka-Goetz M. 2017. The chromatin modifier Satb1 regulates cell fate through Fgf signalling in the early mouse embryo. *Development* **144:** 1450–1461.

Hackett JA, Surani MA. 2014. Regulatory principles of pluripotency: from the ground state up. *Cell Stem Cell* **15:** 416–430. doi:10.1016/j.stem.2014.09.015

Hailesellasse Sene K, Porter CJ, Palidwor G, Perez-Iratxeta C, Muro EM, Campbell PA, Rudnicki MA, Andrade-Navarro MA. 2007. Gene function in early mouse embryonic stem cell differentiation. *BMC Genomics* **8:** 85. doi:10.1186/1471-2164-8-85

Han DW, Tapia N, Joo JY, Greber B, Araúzo-Bravo MJ, Bernemann C, Ko K, Wu G, Stehling M, Do JT, et al. 2010. Epiblast stem cell subpopulations represent mouse embryos of distinct pregastrulation stages. *Cell* **143:** 617–627. doi:10.1016/j.cell.2010.10.015

Hanna LA, Foreman RK, Tarasenko IA, Kessler DS, Labosky PA. 2002. Requirement for *Foxd3* in maintaining pluripotent cells of the early mouse embryo. *Genes Dev* **16:** 2650–2661. doi:10.1101/gad.1020502

Heinz S, Benner C, Spann N, Bertolino E, Lin YC, Laslo P, Cheng JX, Murre C, Singh H, Glass CK. 2010. Simple combinations of lineage-determining transcription factors prime *cis*-regulatory elements required for macrophage and B cell identities. *Mol Cell* **38:** 576–589. doi:10.1016/j.molcel.2010.05.004

Hendriks IA, D'Souza RC, Chang JG, Mann M, Vertegaal AC. 2015. System-wide identification of wild-type SUMO-2 conjugation sites. *Nat Commun* **6:** 7289. doi:10.1038/ncomms8289

Hendriks IA, Lyon D, Su D, Skotte NH, Daniel JA, Jensen LJ, Nielsen ML. 2018. Site-specific characterization of endogenous SUMOylation across species and organs. *Nat Commun* **9:** 2456. doi:10.1038/s41467-018-04957-4

Heurtier V, Owens N, Gonzalez I, Mueller F, Proux C, Mornico D, Clerc P, Dubois A, Navarro P. 2019. The molecular logic of Nanog-induced self-renewal in mouse embryonic stem cells. *Nat Commun* **10:** 1109. doi:10.1038/s41467-019-09041-z

Ignatova VV, Stolz P, Kaiser S, Gustafsson TH, Lastres PR, Sanz-Moreno A, Cho YL, Amarie OV, Aguilar-Pimentel A, Klein-Rodewald T, et al. 2020. The rRNA m^6A methyltransferase METTL5 is involved in pluripotency and developmental programs. *Genes Dev* **34:** 715–729. doi:10.1101/gad.333369.119

Kalkan T, Olova N, Roode M, Mulas C, Lee HJ, Nett I, Marks H, Walker R, Stunnenberg HG, Lilley KS, et al. 2017. Tracking the embryonic stem cell transition from ground state pluripotency. *Development* **144:** 1221–1234.

Kalkan T, Bornelöv S, Mulas C, Diamanti E, Lohoff T, Ralser M, Middelkamp S, Lombard P, Nichols J, Smith A. 2019. Complementary activity of ETV5, RBPJ, and TCF3 drives formative transition from naive pluripotency. *Cell Stem Cell* **24:** 785–801.e7. doi:10.1016/j.stem.2019.03.017

Karvonen U, Jääskeläinen T, Rytinki M, Kaikkonen S, Palvimo JJ. 2008. ZNF451 is a novel PML body- and SUMO-associated transcriptional coregulator. *J Mol Biol* **382:** 585–600. doi:10.1016/j.jmb.2008.07.016

Koidl S, Eisenhardt N, Fatouros C, Droescher M, Chaugule VK, Pichler A. 2016. The SUMO2/3 specific E3 ligase ZNF451-1 regulates PML stability. *Int J Biochem Cell Biol* **79:** 478–487. doi:10.1016/j.biocel.2016.06.011

Krishnakumar R, Chen AF, Pantovich MG, Danial M, Parchem RJ, Labosky PA, Blelloch R. 2016. FOXD3 regulates pluripotent stem cell potential by simultaneously initiating and repressing enhancer activity. *Cell Stem Cell* **18:** 104–117. doi:10.1016/j.stem.2015.10.003

Langmead B, Salzberg SL. 2012. Fast gapped-read alignment with Bowtie 2. *Nat Methods* **9:** 357–359. doi:10.1038/nmeth.1923

Lanner F, Rossant J. 2010. The role of FGF/Erk signaling in pluripotent cells. *Development* **137:** 3351–3360. doi:10.1242/dev.050146

Lee TI, Johnstone SE, Young RA. 2006. Chromatin immunoprecipitation and microarray-based analysis of protein location. *Nat Protoc* **1:** 729–748. doi:10.1038/nprot.2006.98

Lee HY, Johnson KD, Fujiwara T, Boyer ME, Kim SI, Bresnick EH. 2009. Controlling hematopoiesis through sumoylation-dependent regulation of a GATA factor. *Mol Cell* **36:** 984–995. doi:10.1016/j.molcel.2009.11.005

Leone DP, Heavner WE, Ferenczi EA, Dobreva G, Huguenard JR, Grosschedl R, McConnell SK. 2015. Satb2 regulates the differentiation of both callosal and subcerebral projection neurons in the developing cerebral cortex. *Cerebral cortex* **25:** 3406–3419. doi:10.1093/cercor/bhu156

Li M, Belmonte JC. 2017. Ground rules of the pluripotency gene regulatory network. *Nat Rev Genet* **18:** 180–191. doi:10.1038/nrg.2016.156

Li H, Durbin R. 2009. Fast and accurate short read alignment with burrows-wheeler transform. *Bioinformatics* **25:** 1754–1760. doi:10.1093/bioinformatics/btp324

Martello G, Smith A. 2014. The nature of embryonic stem cells. *Annu Rev Cell Dev Biol* **30:** 647–675. doi:10.1146/annurev-cellbio-100913-013116

Mascetti VL, Pedersen RA. 2016. Contributions of mammalian chimeras to pluripotent stem cell research. *Cell Stem Cell* **19:** 163–175. doi:10.1016/j.stem.2016.07.018

Mitsui K, Tokuzawa Y, Itoh H, Segawa K, Murakami M, Takahashi K, Maruyama M, Maeda M, Yamanaka S. 2003. The homeoprotein Nanog is required for maintenance of pluripotency in mouse epiblast and ES cells. *Cell* **113:** 631–642. doi:10.1016/S0092-8674(03)00393-3

Mumbach MR, Rubin AJ, Flynn RA, Dai C, Khavari PA, Greenleaf WJ, Chang HY. 2016. HiChIP: efficient and sensitive analysis of protein-directed genome architecture. *Nat Methods* **13:** 919–922. doi:10.1038/nmeth.3999

Nakagomi K, Kohwi Y, Dickinson LA, Kohwi-Shigematsu T. 1994. A novel DNA-binding motif in the nuclear matrix attachment DNA-binding protein SATB1. *Mol Cell Biol* **14:** 1852–1860.

Neagu A, van Genderen E, Escudero I, Verwegen L, Kurek D, Lehmann J, Stel J, Dirks RAM, van Mierlo G, Maas A, et al. 2020. In vitro capture and characterization of embryonic rosette-stage pluripotency between naive and primed states. *Nat Cell Biol* **22:** 534–545. doi:10.1038/s41556-020-0508-x

Nichols J, Smith A. 2009. Naive and primed pluripotent states. *Cell Stem Cell* **4:** 487–492. doi:10.1016/j.stem.2009.05.015

Niwa H, Ogawa K, Shimosato D, Adachi K. 2009. A parallel circuit of LIF signalling pathways maintains pluripotency of mouse ES cells. *Nature* **460:** 118–122. doi:10.1038/nature08113

Ouyang J, Shi Y, Valin A, Xuan Y, Gill G. 2009. Direct binding of CoREST1 to SUMO-2/3 contributes to gene-specific repression by the LSD1/CoREST1/HDAC complex. *Mol Cell* **34:** 145–154. doi:10.1016/j.molcel.2009.03.013

Paakinaho V, Kaikkonen S, Makkonen H, Benes V, Palvimo JJ. 2014. SUMOylation regulates the chromatin occupancy and anti-proliferative gene programs of glucocorticoid receptor. *Nucleic Acids Res* **42:** 1575–1592. doi:10.1093/nar/gkt1033

Pastor WA, Stroud H, Nee K, Liu W, Pezic D, Manakov S, Lee SA, Moissiard G, Zamudio N, Bourc'his D, et al. 2014. MORC1 represses transposable elements in the mouse male germline. *Nat Commun* **5:** 5795. doi:10.1038/ncomms6795

Quinlan AR, Hall IM. 2010. BEDTools: a flexible suite of utilities for comparing genomic features. *Bioinformatics* **26:** 841–842. doi:10.1093/bioinformatics/btq033

Qureshi IA, Gokhan S, Mehler MF. 2010. REST and CoREST are transcriptional and epigenetic regulators of seminal neural fate decisions. *Cell cycle* **9:** 4477–4486. doi:10.4161/cc.9.22.13973

Ramakrishna S, Kim KS, Baek KH. 2014. Posttranslational modifications of defined embryonic reprogramming transcription factors. *Cell Reprogram* **16:** 108–120. doi:10.1089/cell.2013.0077

Ramírez F, Dündar F, Diehl S, Grüning BA, Manke T. 2014. Deeptools: a flexible platform for exploring deep-sequencing data. *Nucleic Acids Res* **42:** W187–W191. doi:10.1093/nar/gku365

Ramírez F, Bhardwaj V, Arrigoni L, Lam KC, Grüning BA, Villaveces J, Habermann B, Akhtar A, Manke T. 2018. High-resolution TADs reveal DNA sequences underlying genome organization in flies. *Nat Commun* **9:** 189. doi:10.1038/s41467-017-02525-w

Ran FA, Hsu PD, Wright J, Agarwala V, Scott DA, Zhang F. 2013. Genome engineering using the CRISPR-Cas9 system. *Nat Protoc* **8:** 2281–2308. doi:10.1038/nprot.2013.143

Rao SS, Huntley MH, Durand NC, Stamenova EK, Bochkov ID, Robinson JT, Sanborn AL, Machol I, Omer AD, Lander ES, et al. 2014. A 3D map of the human genome at kilobase resolution reveals principles of chromatin looping. *Cell* **159:** 1665–1680. doi:10.1016/j.cell.2014.11.021

Respuela P, Nikolić M, Tan M, Frommolt P, Zhao Y, Wysocka J, Rada-Iglesias A. 2016. Foxd3 promotes exit from naive pluripotency through enhancer decommissioning and inhibits germline specification. *Cell Stem Cell* **18:** 118–133. doi:10.1016/j.stem.2015.09.010

Rhee HS, Closser M, Guo Y, Bashkirova EV, Tan GC, Gifford DK, Wichterle H. 2016. Expression of terminal effector genes in mammalian neurons is maintained by a dynamic relay of transient enhancers. *Neuron* **92:** 1252–1265. doi:10.1016/j.neuron.2016.11.037

Sachs P, Ding D, Bergmaier P, Lamp B, Schlagheck C, Finkernagel F, Nist A, Stiewe T, Mermoud JE. 2019. SMARCAD1 ATPase activity is required to silence endogenous retroviruses in embryonic stem cells. *Nat Commun* **10:** 1335. doi:10.1038/s41467-019-09078-0

Savarese F, Dávila A, Nechanitzky R, De La Rosa-Velazquez I, Pereira CF, Engelke R, Takahashi K, Jenuwein T, Kohwi-Shigematsu T, Fisher AG, et al. 2009. Satb1 and Satb2 regulate embryonic stem cell differentiation and *Nanog* expression. *Genes Dev* **23:** 2625–2638. doi:10.1101/gad.1815709

Schellenberg MJ, Lieberman JA, Herrero-Ruiz A, Butler LR, Williams JG, Muñoz-Cabello AM, Mueller GA, London RE, Cortés-Ledesma F, Williams RS. 2017. ZATT (ZNF451)-mediated resolution of topoisomerase 2 DNA-protein cross-links. *Science* **357:** 1412–1416. doi:10.1126/science.aam6468

Schneider R, Grosschedl R. 2007. Dynamics and interplay of nuclear architecture, genome organization, and gene expression. *Genes Dev* **21:** 3027–3043. doi:10.1101/gad.1604607

Silva J, Nichols J, Theunissen TW, Guo G, van Oosten AL, Barrandon O, Wray J, Yamanaka S, Chambers I, Smith A. 2009. Nanog is the gateway to the pluripotent ground state. *Cell* **138:** 722–737. doi:10.1016/j.cell.2009.07.039

Smith A. 2017. Formative pluripotency: the executive phase in a developmental continuum. *Development* **144:** 365–373. doi:10.1242/dev.142679

Stankovic-Valentin N, Deltour S, Seeler J, Pinte S, Vergoten G, Guérardel C, Dejean A, Leprince D. 2007. An acetylation/deacetylation-SUMOylation switch through a

phylogenetically conserved ψKXEP motif in the tumor suppressor *HIC1* regulates transcriptional repression activity. *Mol Cell Biol* **27:** 2661–2675. doi:10.1128/MCB.01098-06

Subramanian A, Tamayo P, Mootha VK, Mukherjee S, Ebert BL, Gillette MA, Paulovich A, Pomeroy SL, Golub TR, Lander ES, et al. 2005. Gene set enrichment analysis: a knowledge-based approach for interpreting genome-wide expression profiles. *Proc Natl Acad Sci* **102:** 15545–15550. doi:10.1073/pnas.0506580102

Sutinen P, Malinen M, Heikkinen S, Palvimo JJ. 2014. SUMOylation modulates the transcriptional activity of androgen receptor in a target gene and pathway selective manner. *Nucleic Acids Res* **42:** 8310–8319. doi:10.1093/nar/gku543

Theurillat I, Hendriks IA, Cossec JC, Andrieux A, Nielsen ML, Dejean A. 2020. Extensive SUMO modification of repressive chromatin factors distinguishes pluripotent from somatic cells. *Cell Rep* **33:** 108251. doi:10.1016/j.celrep.2020.108251

Torres-Padilla ME, Chambers I. 2014. Transcription factor heterogeneity in pluripotent stem cells: a stochastic advantage. *Development* **141:** 2173–2181. doi:10.1242/dev.102624

Trapnell C, Roberts A, Goff L, Pertea G, Kim D, Kelley DR, Pimentel H, Salzberg SL, Rinn JL, Pachter L. 2012. Differential gene and transcript expression analysis of RNA-seq experiments with TopHat and cufflinks. *Nat Protoc* **7:** 562–578. doi:10.1038/nprot.2012.016

Tsutsui KM, Sano K, Tsutsui K. 2005. Dynamic view of the nuclear matrix. *Acta Med Okayama* **59:** 113–120.

Van Rechem C, Boulay G, Pinte S, Stankovic-Valentin N, Guérardel C, Leprince D. 2010. Differential regulation of HIC1 target genes by CtBP and NuRD, via an acetylation/SUMOylation switch, in quiescent versus proliferating cells. *Mol Cell Biol* **30:** 4045–4059. doi:10.1128/MCB.00582-09

Vougiouklakis T, Nakamura Y, Saloura V. 2017. Critical roles of protein methyltransferases and demethylases in the regulation of embryonic stem cell fate. *Epigenetics* **12:** 1015–1027. doi:10.1080/15592294.2017.1391430

Wang J, Scully K, Zhu X, Cai L, Zhang J, Prefontaine GG, Krones A, Ohgi KA, Zhu P, Garcia-Bassets I, et al. 2007. Opposing LSD1 complexes function in developmental gene activation and repression programmes. *Nature* **446:** 882–887. doi:10.1038/nature05671

Wang Z, Oron E, Nelson B, Razis S, Ivanova N. 2012. Distinct lineage specification roles for NANOG, OCT4, and SOX2 in human embryonic stem cells. *Cell Stem Cell* **10:** 440–454. doi:10.1016/j.stem.2012.02.016

Wang Z, Yang X, Guo S, Yang Y, Su XC, Shen Y, Long J. 2014. Crystal structure of the ubiquitin-like domain-CUT repeat-like tandem of special AT-rich sequence binding protein 1 (SATB1) reveals a coordinating DNA-binding mechanism. *J Biol Chem* **289:** 27376–27385. doi:10.1074/jbc.M114.562314

Weinberger L, Ayyash M, Novershtern N, Hanna JH. 2016. Dynamic stem cell states: naive to primed pluripotency in rodents and humans. *Nat Rev Mol Cell Biol* **17:** 155–169. doi:10.1038/nrm.2015.28

Whyte WA, Bilodeau S, Orlando DA, Hoke HA, Frampton GM, Foster CT, Cowley SM, Young RA. 2012. Enhancer decommissioning by LSD1 during embryonic stem cell differentiation. *Nature* **482:** 221–225. doi:10.1038/nature10805

Wu J, Huang B, Chen H, Yin Q, Liu Y, Xiang Y, Zhang B, Liu B, Wang Q, Xia W, et al. 2016. The landscape of accessible chromatin in mammalian preimplantation embryos. *Nature* **534:** 652–657. doi:10.1038/nature18606

Xiao S, Lu J, Sridhar B, Cao X, Yu P, Zhao T, Chen CC, McDee D, Sloofman L, Wang Y, et al. 2017. SMARCAD1 contributes to the regulation of naive pluripotency by interacting with histone citrullination. *Cell Rep* **18:** 3117–3128. doi:10.1016/j.celrep.2017.02.070

Yamasaki K, Yamasaki T. 2016. The combination of sequence-specific and nonspecific DNA-binding modes of transcription factor SATB1. *Biochem J* **473:** 3321–3339. doi:10.1042/BCJ20160236

Yang Y, Wang Z, Sun L, Shao L, Yang N, Yu D, Zhang X, Han X, Sun Y. 2015. SATB1 mediates long-range chromatin interactions: a dual regulator of anti-apoptotic BCL2 and pro-apoptotic NOXA genes. *PLoS One* **10:** e0139170. doi:10.1371/journal.pone.0139170

Yasui D, Miyano M, Cai S, Varga-Weisz P, Kohwi-Shigematsu T. 2002. SATB1 targets chromatin remodelling to regulate genes over long distances. *Nature* **419:** 641–645. doi:10.1038/nature01084

Ying QL, Stavridis M, Griffiths D, Li M, Smith A. 2003. Conversion of embryonic stem cells into neuroectodermal precursors in adherent monoculture. *Nat Biotechnol* **21:** 183–186. doi:10.1038/nbt780

Zhang Y, Liu T, Meyer CA, Eeckhoute J, Johnson DS, Bernstein BE, Nusbaum C, Myers RM, Brown M, Li W, et al. 2008. Model-based analysis of ChIP-seq (MACS). *Genome Biol* **9:** R137. doi:10.1186/gb-2008-9-9-r137

Zheng M, Xing W, Liu Y, Li M, Zhou H. 2017. Tetramerization of SATB1 is essential for regulating of gene expression. *Mol Cell Biochem* **430:** 171–178. doi:10.1007/s11010-017-2964-6